AD-E300 315

DNA 4534F

TARGET VULNERABILITY AND HARDNESS UNCERTAINTY ANALYSIS

TRW Defense and Space Systems Group
One Space Park
Redondo Beach, California 90278

31 January 1977

Final Report for Period 30 March 1976—31 January 1977

CONTRACT No. DNA 001-76-C-0229

THIS WORK SPONSORED BY THE DEFENSE NUCLEAR AGENCY
UNDER RDT&E RMSS CODE B344076464 Y99QAXSC06206 H2590D.

Prepared for
Director
DEFENSE NUCLEAR AGENCY
Washington, D. C. 20305

Destroy this report when it is no longer needed. Do not return to sender.

PLEASE NOTIFY THE DEFENSE NUCLEAR AGENCY, ATTN: TISI, WASHINGTON, D.C. 20305, IF YOUR ADDRESS IS INCORRECT, IF YOU WISH TO BE DELETED FROM THE DISTRIBUTION LIST, OR IF THE ADDRESSEE IS NO LONGER EMPLOYED BY YOUR ORGANIZATION.

(18) DNA, SBIE (19) 4534 F, AD-E300 315

UNCLASSIFIED

SECURITY CLASSIFICATION OF THIS PAGE (When Data Entered)

REPORT DOCUMENTATION PAGE		READ INSTRUCTIONS BEFORE COMPLETING FORM
1. REPORT NUMBER DNA 4534F	2. GOVT ACCESSION NO.	3. RECIPIENT'S CATALOG NUMBER
4. TITLE (and Subtitle) (6) TARGET VULNERABILITY AND HARDNESS UNCERTAINTY ANALYSIS		5. TYPE OF REPORT & PERIOD COVERED (9) Final Report, for Period 30 Mar 76—31 Jan 77
		6. PERFORMING ORG. REPORT NUMBER 29426-6001-RU-00
7. AUTHOR(s) (10) John J. Farrell, Juen S. Chiu, Norman Lipner, Augusto L. Soux		8. CONTRACT OR GRANT NUMBER(s) (15) DNA 001-76-C-0229
9. PERFORMING ORGANIZATION NAME AND ADDRESS TRW Defense and Space Systems Group, One Space Park, Redondo Beach, California 90278		10. PROGRAM ELEMENT, PROJECT, TASK AREA & WORK UNIT NUMBERS NWED Subtask Y99QAXSC062-06
11. CONTROLLING OFFICE NAME AND ADDRESS Director, Defense Nuclear Agency, Washington, D.C. 20305		12. REPORT DATE (11) 31 January 1977
		13. NUMBER OF PAGES 96
14. MONITORING AGENCY NAME & ADDRESS (if different from Controlling Office) (16) Y99QAXS		15. SECURITY CLASS. (of this report) UNCLASSIFIED
		15a. DECLASSIFICATION/DOWNGRADING SCHEDULE

16. DISTRIBUTION STATEMENT (of this Report) (17) C062

Approved for public release; distribution unlimited. (12) 87p.

17. DISTRIBUTION STATEMENT (of the abstract entered in Block 20, if different from Report)

(14) TRW-29426-6001-RU-00

18. SUPPLEMENTARY NOTES

This work sponsored by the Defense Nuclear Agency under RDT&E RMSS Code B344076464 Y99QAXSC06206 H2590D.

19. KEY WORDS (Continue on reverse side if necessary and identify by block number)

Target Hardness	Nuclear Weapon Effects
Uncertainty	Industrial Buildings
Structural Response	Shallow Buried Bunkers

20. ABSTRACT (Continue on reverse side if necessary and identify by block number)

Large uncertainties on target vulnerability and hardness have influenced U.S. strategic targeting and R&D planning. The objective of this study was to develop quantitative methods for analyzing uncertainty in target vulnerability and hardness predictions. Methods for target hardness predictions and the analysis of the associated uncertainty given good intelligence, were evaluated for application to two targets, namely, 1) above-ground industrial building; and 2) shallow-buried command and control bunker. → next page

DD FORM 1473, 1 JAN 73 EDITION OF 1 NOV 65 IS OBSOLETE

78 08 03 20

UNCLASSIFIED

SECURITY CLASSIFICATION OF THIS PAGE (When Data Entered)

407 637

20. ABSTRACT (Continued)

cont.

The procedure for evaluating target hardness uncertainty was started with the formulation of mathematical models of the weapon effects and the target response and failure. Structural responses models for both targets were developed based on classical structural dynamics considerations. However, for the buried bunker, the structural model is more uncertain because of the inadequate data base. Uncertainties on model parameters were characterized and propagated through the analysis using a Taylor-series expansion method, to evaluate the best estimate hardness and the hardness uncertainty as a function of weapon yield. The results were evaluated and compared with the Physical Vulnerability System.

PREFACE

This report, "Target Vulnerability and Hardness Uncertainty Analysis" was supported by the Defense Nuclear Agency under Contract No. DNA-001-76-C-0229, Program Element NWE D62704H Project Y99QAXS Task Area C062 Work Unit 06. The period covered is from 30 March 1976 through 31 January 1977.

The study was conducted by personnel of Ground Systems and Technology Department of TRW Defense and Space Systems Group under the general direction of Dr. Peter K. Dai. The authors are grateful for the helpful suggestions of Dr. Kent L. Goering, Technical Monotor DNA/SPSS, and are indebted to Dr. Henry F. Cooper and Mr. Robert J. Port of R&D Associates for their useful discussions of target vulnerability. The authors also wish to thank Dr. Paul F. Hadala of Waterways Experiment Station for the data which he supplied to us on the buried bunker.

The authors also acknowledge the contributions of Dr. Robert E. Hutton and Dr. David S. Liu to the industrial building analysis and the contributions of Dr. Paul Chen and Mr. Gary M. Teraoka to the buried bunker analysis, and of Mr. Leo H. Donahue to the final report.

Conversion Factors for U.S. Customary
to Metric (SI) Units of Measurement

To convert from	To	Multiply by
mils	millimeters	0.0254
inches	centimeters	2.54
feet	meters	0.3048
miles	kilometers	1.6093
square inches	square centimeters	6.4516
square feet	square meters	0.0929
square miles	square meters	2,589,998.0
cubic inches	cubic centimeters	16.38706
cubic feet	cubic meters	0.0283
cubic yards	cubic meters	0.764555
gallons (U.S.)	liters	3.785
gallons (Imperial)	liters	4.542
ounces	grams	28.349
pounds	kilograms	0.454
tons (short)	kilograms	907.185
tons (long)	kilograms	1,016.047
pounds per foot	newtons per meter	14.59390
pounds per square inch	newtons per square centimeter	0.6894757
pounds per cubic inch	kilograms per cubic centimeter	27,679.90
pounds per square foot	newtons per square meter	47.88026
pounds per cubic foot	kilograms per cubic meter	16.0185
inches per second	centimeters per second	2.54
inch-pounds	meter-newtons	0.1129848
inch-kips	meter-kilonewtons	0.0001129848
Fahrenheit degrees	Celsius degrees or Kelvins[a]	
kilotons	terajoules	4.183

[a]To obtain Celsius (C) temperature readings from Fahrenheit (F) readings, use C = (5/9)(F-32). To obtain Kelvin (K) readings, use K = (5/9)(F-32) + 273.15.

TABLE OF CONTENTS

LIST OF FIGURES

LIST OF TABLES

1. INTRODUCTION

A methodology for systematically evaluating the uncertainties associated with the prediction of vulnerability and hardness of ground facilities has been used for the past ten years to develop confidence statements, from the defender's point of view, for weapon systems survivability prediction. In this application, the defender theoretically has perfect intelligence of site conditions and structural configurations and materials, and can establish, analytically or experimentally, the weapon effect environments and structural fragilities to within acceptable uncertainty bounds. Parametric sensitivity analyses are conducted to evaluate the impact of various uncertainties on the system survivability. This information proves to be invaluable for conducting design trade-offs, and for weapon effects research planning.

The present study represents the first attempt to apply such a methodology to analyzing the uncertainties in target vulnerability and hardness predictions. Target vulnerability and hardness and associated uncertainties, given good intelligence, were evaluated for two representative targets: (1) an above-surface industrial building; and (2) a shallow-buried command and control bunker.

The procedure for evaluating target hardness uncertainty was started with the formulation of mathematical models of the weapon effects and the target response and failure. Structural responses models for both targets were developed based on classical structural dynamics considerations. However, for the buried bunker, the structural model is more uncertain because of the inadequate data base. Uncertainties on model parameters were characterized and propagated through the analysis using a Taylor-series expansion method, to evaluate the best estimate hardness and the hardness uncertainty as a function of weapon yield. The results were evaluated and compared with the Physical Vulnerability System.

Uncertainties caused by potential systematic errors of analysis, i.e., bias between the mathematical model and the real world, were distinguished from nonsystematic, random variations of physical properties. When propagated through the weapon effect scaling laws, nonsystematic variations lead to variations in estimated damage distances. These nonsystematic damage distance variations are treated adequately by the Physical Vulnerability System, and for most cases do not cause significant errors in the estimated damage probabilities. However, systematic errors in target hardness estimates cause systematic errors in estimated damage probabilities which are not treated adequately by the Physical Vulnerability System at present. The emphasis of this study is focused upon the problems of quantifying the effects of the systematic errors of analysis.

From the results, it was concluded that for above surface targets such as industrial buildings, the current procedure for determining the best estimate of physical vulnerability is adequate. Uncertainty in the target physical vulnerability can be quantified based on the state-of-the-art knowledge of low level blast environments, material properties, and structural response modeling. Scale model tests of industrial targets would not be worthwhile unless the structural models were accurate representations of a high-value class of uniformly constructed structures.

For the shallow-buried targets such as command bunkers, procedures for physical vulnerability prediction to achieve the desired confidence levels remain to be validated. Of significant uncertainty is the structural response model and failure criteria. Testing of model structures to failure with the objective of developing more accurate prediction techniques is recommended. Additional sensitivity analyses, and research cost-benefit trade-off studies should be conducted to provide a basis for setting priority for research projects pertinent to bunker vulnerability.

2.0 STUDY APPROACH

Target hardness predictions are generally derived analytically, and the uncertainties in these predictions are dependent upon the inputs to the analysis, and also upon the analytical model itself. In the present study, mathematical models for nuclear weapon environments and target structural loads and response were developed as a first step. The sources of uncertainties in the model parameters were then identified, and nominal values and uncertainty bounds for these parameters were determined. The analytical models were used to determine both target hardness predictions, and the sensitivity of these predictions to perturbations within the uncertainty bounds of the parameters input to the models. Next, the uncertainties of the parameters were propagated through the structural response model to determine the uncertainty bounds on the target hardness estimates. The final and most difficult step in the quantification of the target hardness uncertainty was to estimate the accuracy of the mathematical model itself, and incorporate this information into the target hardness estimate.

Section 2.1 discusses the distinction between random variations and uncertainties, and how these quantities are defined. The methodology for calculating hardness uncertainties, and the impact of these uncertainties on targeting is given in Section 2.2.

2.1 STATISTICAL CONSIDERATIONS

If a number of cylinders, cast from the same batch of concrete and cured in a carefully controlled manner, were subjected to an unconfined compression test in the same loading device at essentially the same time, identical resistance would not be exhibited by each cylinder. Individual differences in the cylinders, such as air voids in the concrete, which occur randomly and can never be completely eliminated, would cause cylinder-to-cylinder strength variations. Thus, the strength of cylinders cast from a single batch of concrete is a random variable. Random variations are the actual physical variations that occur within a group, such as cylinders cast from the same batch of concrete, or from the same concrete mix specifications.

When a specific cylinder is considered, the unconfined compressive strength is not a random variable, since it has one specific, true value. This true value can be estimated, for example, based on a knowledge of the properties of the concrete batch from which it was cast. However, such an estimate will vary from the true value of strength of this particular cylinder because of random variation among cylinders from the batch. The true value of the unconfined compressive strength of a particular cylinder can be determined by subjecting the cylinder to a compression test.

Even after the test has been performed, there remains some uncertainty in the result. This determination of the true value of the compressive strength of the cylinder is only as good as the accuracy of the test will permit. Errors in the test measurements will cause an error in the determination of the true value of the cylinder strength. In many cases, this uncertainty can have more impact on the outcome of a study than the random variations. Effects of random variations tend to be self cancelling, while uncertainty often adds a significant error to the entire study result.

Uncertainty refers to potential differences between the real world and the perceived world of analytical models and of model parameter values. There will be uncertainty in the measure of central tendency of a random variable (for example, the mean or median value), in the measure of its spread (for example, the standard deviation), and in the distribution function selected for the variable. The uncertainty in any of these statistical properties is the confidence, or the expectation, that the true parameter value is less than a specified value, defined over the range of possible values. (A 50% confidence value implies that the actual parameter value is as likely to be higher as it is to be lower). Uncertainty in the measure of central tendency of a targeting analysis variable, or in the analytical model chosen could introduce significant uncertainty in the targeting analysis results. However, uncertainties in the variance or in the distribution function of an analysis variable are generally not significant.

The bounding values of a variable, or the limiting responses associated with the extremes of model assumptions, are the usual bases for estimating uncertainties. There is necessarily a degree of subjectivity on the confidence level ascribed to bounds. Reasonable engineering bounds are sometimes taken to represent 95% confidence bounds. Thus, if the uncertainty in the variable under consideration is normally distributed, these bounds will correspond to a region within plus-and-minus two standard deviations from the mean.

In targeting analysis both random variation and uncertainty effects should be properly treated. The response of a specific concrete structure, subjected to the effects associated with a particular nuclear device detonated at a specific location and time, is deterministic. There will be uncertainty, but not random variation, in the response. This is true even though some parameters of the analysis model might be described in terms of both a random variation and an uncertainty distribution, as for example, when the concrete mix specifications are known, but cylinder test data for the actual pour are not available. The random variance associated with the mix strength actually represents an uncertainty on the cylinder strength of the concrete in the specific structure of interest. The effect of this uncertainty is combined with that of other sources of uncertainty to determine the total uncertainty in the target hardness.

Where there are many similar structures constructed using the same mix specifications, the random variation in mix strength will have a smaller effect on the uncertainty in the median structure response if all structures are subjected to similar nuclear loading conditions. Random variation in concrete strength causes some structures to be stronger, and others to be weaker. This variation tends to average out when the median response of a large number of structures is considered. Thus, when analyzing many structures, random variation and uncertainty cannot be combined. Since the random variations tend to be dominated by the weapon miss distance (CEP) distribution, their effects are generally not critical.

An appreciation of the distinction between random variation and uncertainty leads to better understanding of the research options available, in addition to aiding the understanding of complex targeting situations. For example, the ratio of the standard deviations of the uncertainty and the random variations will influence the number of tests required to reduce the uncertainty to an acceptable level.

In the present study, random variations in the analysis parameters are assumed to cause only random variations in the system response. However, it is possible that the effects of random parameter variations around the median conditions will not average out, even after a large number of similar structures are considered. If this were the case, a systematic bias would be introduced in the response. For example, if a group of buried structures have a very stiff median foundation modulus, those sites with higher than median stiffness might exhibit nearly the same response as the median site, i.e., the response associated with a rigid foundation. However, those sites with much lower stiffness could have a markedly different response caused by a rigid body mode. The interaction between random variations and uncertainties can possibly be removed by categorizing sites, such that the response phenomenology is the same for all sites in a category, and by performing separate targeting analyses for each category. However, this interaction is treated in more formal statistical survivability modeling, such as in the FAST code (Reference 1).

Another approximation used in this study is that the uncertainty distributions are assumed to be lognormal. This assumption is commonly used in weapon effects analysis because it conveniently approximates much of the data. If there are a number of uncertain parameters in the system, and these parameters are multiplicative factors affecting the system response, then the Central Limit Theorem indicates that these uncertainties will be lognormally distributed (Reference 2).

Consistent with the assumption of a lognormal distribution, best estimate values of the parameters are taken as the median value of the distribution. For a continuous variable, the median is defined as the value of the variable at which 50% of the area under the distribution function lies above the median, and 50% below. For a lognormal distribution, the median corresponds to the mean of the logarithm of the variable. Uncertainties are defined in terms of 2σ K-factors which represent approximately 95% bounds. This means there is approximately a 95% expectation that the true value of the parameter will be within a factor of K and 1/K of the median value of the parameter. The K-factor is related to the standard deviation of the distribution of the logarithm of the variable by

$$2\sigma = \ln K \tag{2-1}$$

2.2 EVALUATION OF UNCERTAINTIES

Two primary factors determine the importance of the uncertainties in various parameters affecting target response: (1) the sensitivity of the target hardness, p, to uncertainties in the input parameters, x_i; and (2) the uncertainty in the median values of the parameters. If the target hardness is written as

$$\ln p = f(\ln x_i) \tag{2-2}$$

then from Reference 2 (Equation 4.39), the standard deviation in the uncertainty of ln p, σ_{p_j}, which is caused by the uncertainty in the particular parameter, x_j, can be computed from the approximate relationship

$$\sigma_{p_j} = \frac{\partial(\ln p)}{\partial(\ln x_j)} \sigma_j \tag{2-3}$$

where the partial derivative gives the sensitivity of the target hardness to variations in x_j and σ_j is the standard deviation in the uncertainty of ln x_j. The approximation arises from neglecting terms higher than first order in the Taylor-series expansion of the function, f, used in calculating the standard deviation. Then, from Equation (2-1)

$$\ln K_{pj} = \frac{\partial(\ln p)}{\partial(\ln x_j)} \ln K_j \tag{2-4}$$

where K_{pj} and K_j are the uncertainty factors corresponding to σ_{pj} and σ_j, respectively. Continuing with the approach of Reference 2 (Equation 4.44), an expression for the total target hardness uncertainty factor, K_p, can be derived as

$$K_p = \exp\left(\sum_{i=1}^{n}\sum_{j=1}^{n}\rho_{ij}\ \ln K_{pi}\ \ln K_{pj}\right)^{1/2} \qquad (2\text{-}5)$$

where the ρ_{ij} are the correlation coefficients between the target hardness uncertainty factors.

Equations (2-4) and (2-5) make possible the evaluation of the relative impact of the parameter uncertainties on the target hardness uncertainty. In addition, the potential benefits in reduced target hardness uncertainty, resulting from reducing the uncertainties in the key parameters can be readily evaluated with these expressions. Whether these uncertainties can be reduced by test must be determined by a separate evaluation of the potential errors associated with the available test techniques. If no suitable techniques exist, then the requirements for simulation capability can be stated in terms of the needed uncertainty reduction.

To determine the need for uncertainty reduction, the target hardness uncertainties are propagated through the scaling laws for weapon effects to determine damage-distance relationships, and the corresponding uncertainties, as a function of yield. Then, the impact of these uncertainties on the yield and accuracy requirements of the attacker can be evaluated.

For this study, each target was considered to be the object of a single attack aimed directly at that target. Each target was one of many constructed from the same designs and sited in the same generic geology. Therefore, random variations in as-built material properties are about 15 to 30%, and construction tolerances are usually small. For a given generic geology, weapon effect variations are also small, even considering the effect of weather conditions (which are partially known), and total random variation on target damage distances will usually have a standard deviation (σ_D) less that 20% of the median damage distance ($\overline{R}$). Based on the detailed analysis of Reference 3, (Appendix B), the probability of damage, P_K, is very nearly the same as the cookie cutter equation:

$$P_K \approx 1 - P_{cc} \qquad (2\text{-}6)$$

if $P_K \leq 0.9$ and $\sigma_D \leq 0.2\overline{R}$. The cookie cutter approximation is that there is zero probability of failure at ranges greater than $\overline{R}$ and unity at ranges closer-in than $\overline{R}$. Then, convoluting this damage-distance model with the weapon miss distance Rayleigh distribution gives

$$P_{cc} = \exp(-0.5\bar{R}^2/\sigma^2) \qquad (2\text{-}7)$$
$$\sigma = 0.849 \text{ CEP}$$

A property of the Rayleigh distribution is that there is a 50% probability of the weapon landing within a distance from the target equal to the CEP (circular probable error).

The random physical variations do not significantly affect the probability of damage computation in the above case. Their effect is much smaller than that caused by random variation of weapon miss distance (the CEP distribution). On the other hand, a systematic uncertainty in a damage distance estimate does affect the confidence in the calculated probability of damage.

The attacker's confidence (expressed as a function of damage distance) is the expectation that uncertainties in the targeting analysis would not result in a damage distance greater than a given value. Confidence estimates are thus based on the systematic uncertainty in damage distance, assuming a lognormal distribution of the uncertainty. The kill probability as a function of confidence level may be determined from Equation (2-6), using this damage distance versus confidence level distribution.

3.0 INDUSTRIAL TARGET

This section describes the analysis of a typical heavy steel frame industrial building, as shown in Figure 3-1, subjected to dynamic pressure loading. A generalized, single-degree-of-freedom model was utilized because of its tractability and because it has been widely accepted as a useful engineering tool. Work hardening of the structural material was taken into account to arrive at a realistic model for structural behavior. The analysis considers two loading conditions; side-on and end-on. Side-on loading deforms columns and crane rail beams, while end-on loading causes rotation and drop of the crane itself.

Uncertainties in the details of construction of the building, in the loads induced in the structure, and in the response of the structure to these loads are estimated, and propagated throughout the analysis. The magnitude of the uncertainties result in various levels of confidence in the success of an attack. Weapon yield and accuracy requirements are also determined.

3.1 TARGET DESCRIPTION

The target selected for this study (Figure 3-1) is a typical medium size industrial building, as described in Reference 4. It is a single-story, single-span, multi-bay building with a heavy steel frame designed for an industry involving heavy equipment and the manufacture of large products. The typical span length for this class of building is 80 ft and the bay size is about 40 ft. A 50-ton, column-and-girder-supported travelling crane is mounted on beams, bridging the span of the buildings. Steel columns, built up from rolled steel sections, carry the roof and crane loads, and either concrete or steel roof trusses support the main roof load carrier. The joists on both the top and bottom chords are braced to prevent lateral buckling.

Precast reinforced concrete foundations provide seats for the columns. When the column is inserted and fastened, this joint can carry moments transferred from the columns. The foundations extend about six feet below the finished grade to prevent frost action during winter. The crane support girders are rolled steel beams or steel plate girders. The walls are supported by the foundation beams which bridge the span between column foundations. From the ground level up to about ten feet above the ground, the walls are made of brick or large concrete blocks. Above this height, the walls are made of light weight concrete panels or asbestos-cement corrugated sheeting. Commonly used roofing materials are steel sheet, asbestos-cement, and tile.

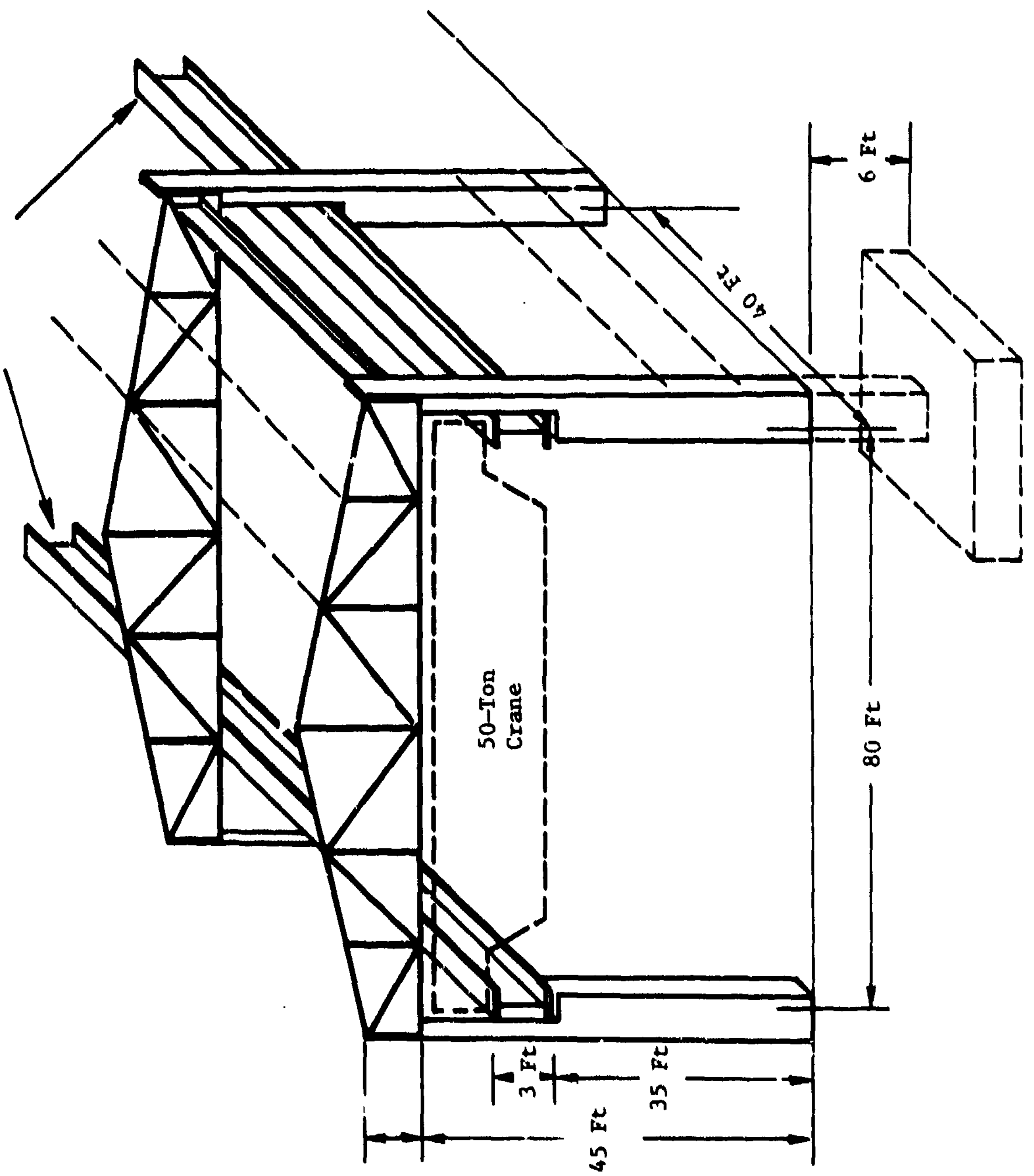

Figure 3-1. Industrial Building Model

3.2 STRUCTURAL RESPONSE ANALYSIS

When the building described in Section 3.1 is subjected to a nuclear attack, several vulnerabilities are possible. However, dynamic pressure and ground shock are the most critical weapon effects for above-the-surface structures. Overpressure and radiation would, of course, be lethal to personnel inside the building, but are not likely to cause permanent damage. Overpressure propagates to the inside of a building of this type faster than structural response, minimizing the effect of differential overpressure between the inside and the outside. At the overpressure levels of interest, structural materials are not affected by radiation, and cratering, debris, and thermal radiation are not significant threats to the building integrity. Electromagnetic pulse might damage electrical equipment and controls, but they can probably be repaired in a few days, or means can be found to operate without them.

Dynamic pressure acts on the side or end of the building like a hurricane, producing a lateral force proportional to the exposed area. Ground shock produces oscillating motions, much like an earthquake, which result in loads dependent on the building mass, and possibly cause differential settlement of columns. Dynamic pressure is the most significant loading mechanism for a building of this type, since there is a relatively large area exposed to the wind, and a relatively small roof mass. Building and crane-beam damage resulting from dynamic pressure are, therefore, the prime failure modes for the industrial building under consideration when subjected to a nuclear attack.

If parts of the roof or siding are blown off by nuclear wind pressure, emergency repairs could be made to permit resumed operations within a few days. However, structural damage to the crane or its supporting structure is likely to require materials which are in short supply in a war situation, and extensive fabrication and erection of major structural members. It was assumed that use of the crane is essential to the industrial process carried on within the building, and that rendering the crane inoperative is a suitable measure of a successful attack.

One mode of failure for the overhead crane may be lateral displacement of the crane rail beams, just enough to allow the crane to fall, while not necessarily exceeding the beam yield stress. Another failure mode may involve substantial plastic deformation of the beams. Based on these failure modes, two limiting attack conditions can be considered: a low level attack of sufficient intensity to produce a lateral beam deflection just large enough to allow the crane to drop, provided it is parked at the location where the maximum lateral deformation occurs; or a higher level attack in which the maximum plastic deflection of the beam has been exceeded, causing the beam to fail, and drop the crane from any parking position along the rail beam.

The geometry of a typical industrial building suggests that two primary loading orientations should be considered, side-on and end-on. For the side-on case, the detonation point is located to the side of the building, but not necessarily centered between the columns. This orientation primarily loads the sides of the building, with a much smaller load on the ends of the building.

In the side-on loading case, the siding is assumed to fail first, since it is not designed to support large side pressures across the span between columns. This leaves the columns and crane rail beams exposed to the dynamic blast pressure. Parts of the siding, however, might stay on the beams and columns increasing the exposed area and, therefore, the load. Such loadings tend to move the rail beams out from under the crane, permitting the crane to fall.

For the end-on loading case, the detonation point is located in front of the building, not necessarily centered, so as to give the major loading to the end with a smaller loading acting on the sides of the building. In this loading case, blast pressures act over the side of the crane. Even though such loadings could subject the crane to pressures which are essentially uniform along its length, yaw moments would be created because of the unsymmetrical frontal area exposed to the blast wave. Such moments induced yaw rotation, which may be large enough to rotate the ends of the crane off the rail beams allowing the crane to fall to the floor.

The free field equations used to determine the loads are given in Appendix A. Uncertainties in the modeling, the loads, and the basic variables are discussed in Section 3.3. The models synthesized to represent side-on and end-on loading of the building are discussed in the following sections, with details given in Appendices B to D.

3.2.1 Side-on Loading

Side pressure on the industrial building will cause rotation of the foundations, bending of the columns as cantilevers, and lateral bending of the beams. The model of the building used in this study consists of two vertical columns attached to the ground through flexible torsional spring support. The rail beam spanning the distance between the tops of the columns has support stiffness between simple and clamped support conditions. The top of the column is assumed to carry a portion of the roof mass. When these structural elements are subjected to the dynamic pressure loading, bending and rotation are induced in the vertical columns and the horizontal rail beams.

The structural response is determined by first approximating the actual system

by the elasto-plastic, single-degree-of-freedom system model, whose governing equations are summarized in Appendix B. In this model, the generalized mass, stiffness, and force are related to the mass and elastic properties of the building, and the dynamic pressure loadings acting on it, by the equations developed in Appendix C.

After the system peak response to a given attack condition was determined, two failure boundaries were computed. The first failure boundary was based on the elastic lateral deformation of the beam just sufficient to allow the crane to fall, if it was located midway between the columns where the maximum lateral displacements occurred. The second failure boundary was based on the maximum stress in the beam exceeding the plastic failure stress, which would cause crane damage regardless of its location.

Figure 3-2 shows the damage distances for both failure criteria, based on the set of median analysis parameters, given in Appendix C. It is seen that there could be a significant enhancement in lethal radius if the crane were parked midway between columns. However, in the vulnerability analysis it was assumed that the crane was parked in its hardest position, near a column, and the plastic failure stress criterion governed. This assumption is reasonable for targeting since the parking position would not be expected to be known.

3.2.2 End-on Loading

Figure 3-3 shows the approximate failure boundary for the end-on loading case. This loading case makes use of a simpler model to determine when crane drop will occur. In the development of the model, it was assumed that the end wall will be destroyed, and the dynamic pressure will act on the face of the crane itself. The dynamic pressure will move the crane along the rail support beams, and at the same time induce a yaw rotation which will tend to rotate the ends of the crane off the rail beams until it falls to the floor. This yaw rotation induced by the dynamic pressure is a consequence of the lack of symmetry in exposed area and loading on the crane. The failure boundary in this case could be based on the actual crane rotation, and the rotation required to cause the crane to fall between the two rail beams at each end of the crane. However, it takes only a relatively small rotation for the crane to be free to fall. Therefore, the failure boundary was approximated by assuming the peak disturbance yaw moment to be equal to the peak resistance yaw moment produced by forces at the crane-rail beam interfaces. A detailed description of the model and the median values of the parameters used is given in Appendix D.

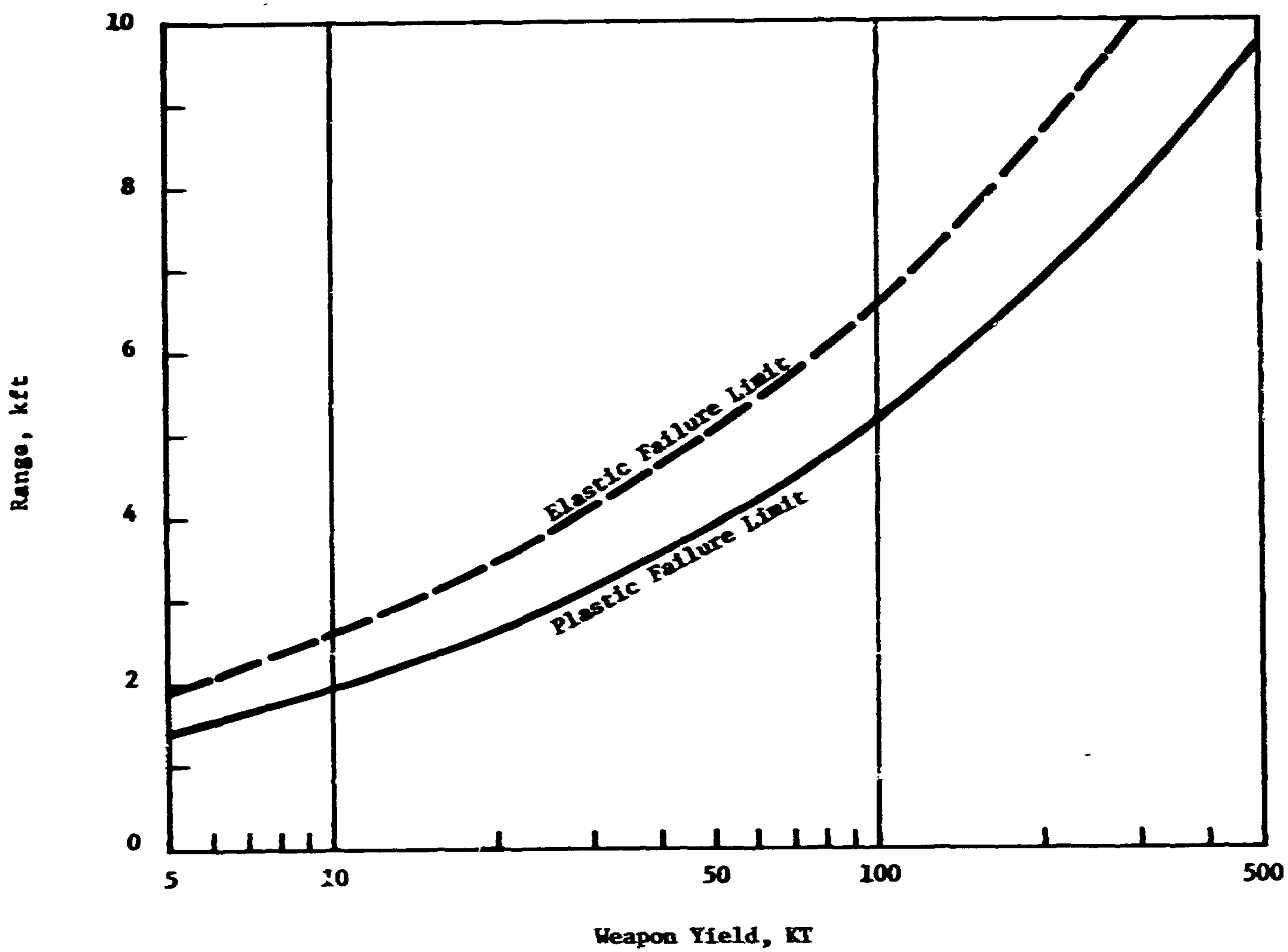

Figure 3-2. Variation of Range With Weapon Yield at Failure
(Side-on Loading Case)

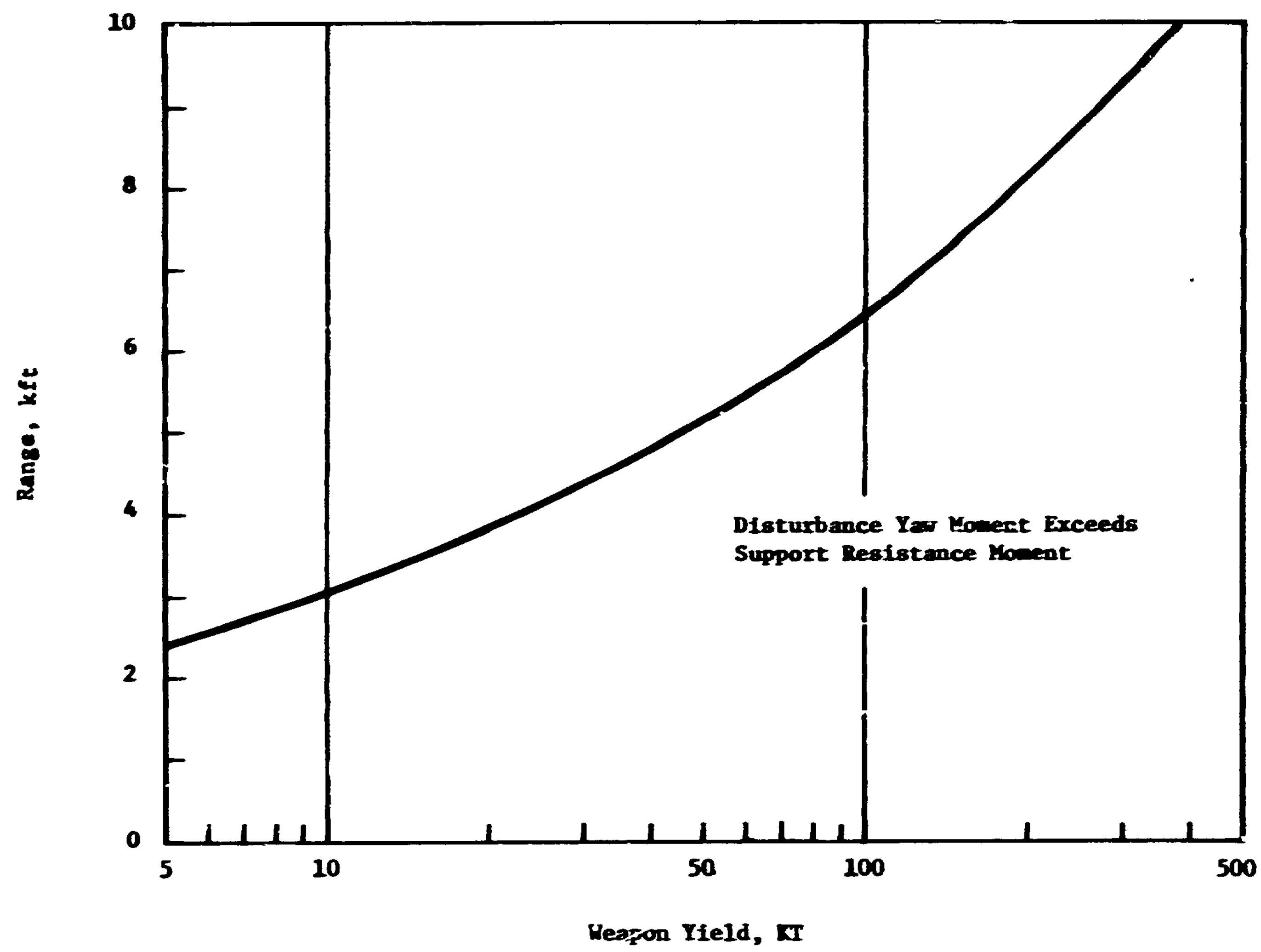

Figure 3-3. Variation of Range With Weapon Yield at Failure (End-on Loading Case)

3.3 STRUCTURAL RESPONSE UNCERTAINTIES

From the attacker's point of view, uncertainties leading to various degrees of confidence in a successful attack on the industrial target may be grouped as follows: uncertainties in weapons effects, uncertainties in intelligence data, and imperfect modeling. In the analysis which follows, these uncertainties are combined with the random distribution of miss distances to obtain probabilities of successful attacks at various confidence levels. To provide a better comparison with World War II damage from Japan, the building in this analysis was assumed to be oriented side-on where the damage criterion is structural failure of the rail beam.

3.3.1 Uncertainty in Loads

The empirical relationships between overpressure and range for a given weapon size have been well established from weapon tests at the Nevada Test Site and the Pacific Proving Ground. The dynamic pressure relationships are not so well defined empirically. The procedure used in this study was to estimate overpressures from the empirical Brode equation, and then compute the dynamic pressure by means of the Rankine-Hugoniot equation (See Appendix A). Overpressures were calculated with a 2-σ uncertainty range of 1.2. A 2-σ uncertainty range of 1.2 means that, if the overpressure uncertainties are lognormally distributed, about 95% of the overpressure values are expected to fall within the range of median/1.2 to median x 1.2.

3.3.2 Uncertainties in Intelligence Data

Intelligence data on targets of interest is necessarily uncertain. This category includes the dimensions, thicknesses, and other properties of the various structural elements. The uncertainties due to intelligence limitations utilized in this study for purposes of illustration are as follows:

Parameter	2σ Uncertainty Factor
Beam	
Moment of Inertia	2.0
Depth	1.2
Weight	1.3
Column	
Moment of Inertia	1.7
Frontal Depth	1.0
Weight	1.5
Roof	
Mass	2.2

3.3.3 Uncertainty in Target Model and Response

Even if the building's characteristics were perfectly known, response predictions to a given dynamic pressure would have large associated uncertainties. The single-degree-of-freedom approximation used here has been widely accepted as a useful engineering model. Predictions based on this model provide engineering estimates in the linear deformation range. Beyond the yield point, however, predictions are less accurate, since the behavior of engineering structures up to total collapse is difficult to predict. Other uncertainties included in this category are the degree of fixity afforded by joints, the drag coefficients associated with the various shapes, and the amount of wall siding that might stay attached to columns and beams, increasing their exposed area. The modeling uncertainties considered in this study are as follows:

Parameter	2σ Uncertainty Factor
Beam	
Drag Coefficient	1.8
End Fixity	3.2
Area Factor	2.2
Column	
Drag Coefficient	1.8
End Fixity	3.2
Area Factor	2.2
Ductility	3.0
Work Hardening Parameter	3.2

3.3.4 Uncertainty Propagation

Figure 3-4 shows the uncertainty in target hardness, in terms of the peak dynamic pressure that causes failure (Q), which results from the uncertainties discussed above. The data for this figure were obtained by expanding the expression for dynamic pressure at failure about the means of the various parameters in a Taylor series, and truncating the series to the linear terms. The resulting expression for the variance of Q involves its partial derivatives with respect to each parameter and the uncertainty of the parameter. The derivatives were calculated numerically, since there is no closed form expression for Q. Assuming a lognormal distribution for Q, 10 and 90% confidence levels were calculated for the range of weapon yields of interest and were plotted in Figure 3-4. A 90% attacker's confidence means that there is a 90% probability that the true (but unknown) hardness is equal to or less than the stated value.

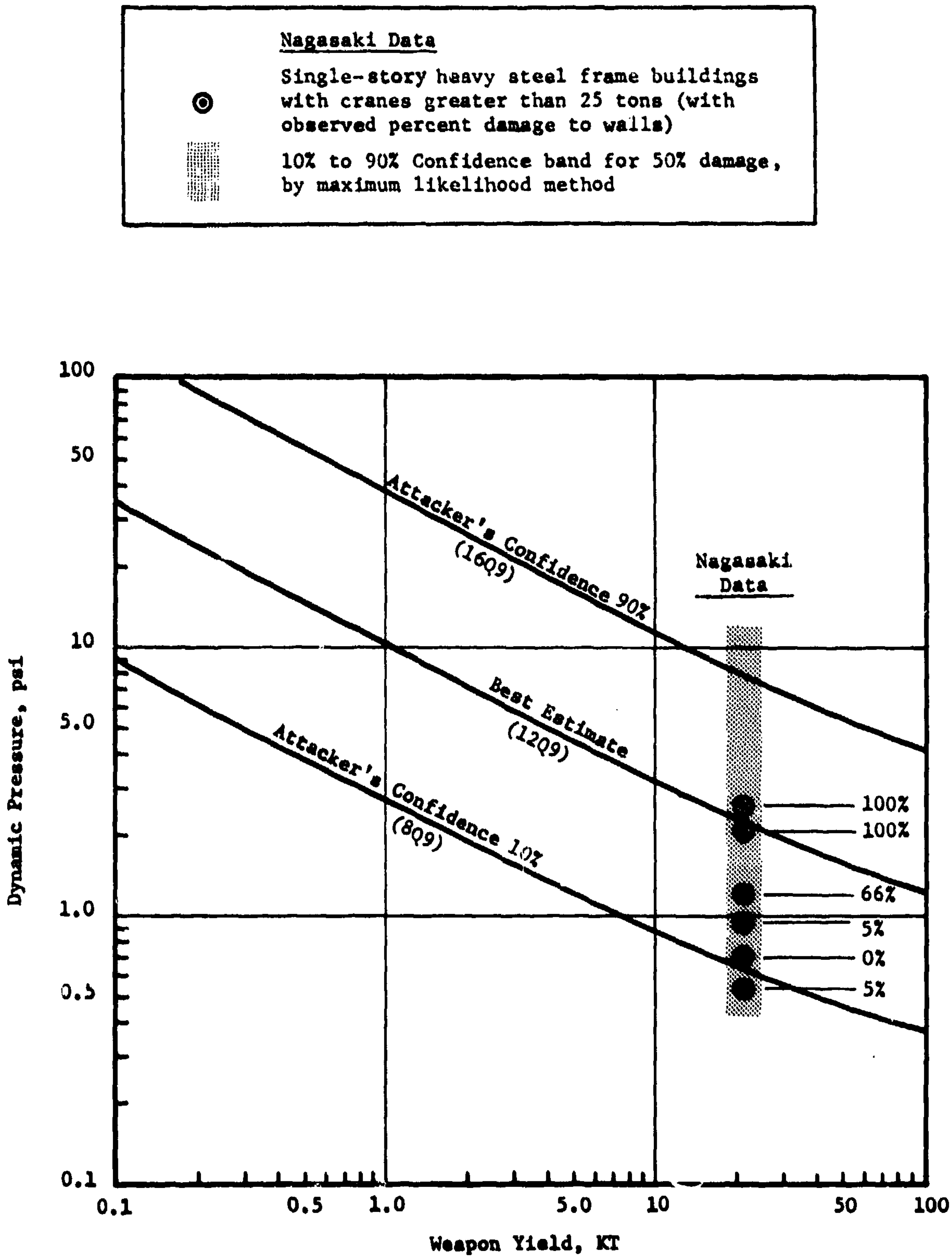

Figure 3-4. Target Hardness

Also shown in Figure 3-4 is a comparison between these analytically derived data, and the actual damage incurred by similar buildings due to the nuclear detonations in Japan during World War II. A recent DNA-sponsored study by Lulejian (Reference 5) has provided a detailed classification and analysis of the damage data compiled by survey teams at the detonation sites in Hiroshima and Nagasaki.

The structural damage to the Japanese buildings was reported in terms of the fraction of damage to the walls and to the roofs of the buildings and the distance of the building from the detonation. For this comparison, the structural damage to the building walls most nearly parallels the measure of building vulnerability used in the present study.

The data base includes 41 single-story heavy steel frame buildings, 38 in Nagasaki and only three in Hiroshima. These buildings are divided into two groups, those with cranes less than 25 tons, and those with cranes greater than 25 tons. The single-story buildings with heavy cranes comparable to the industrial target studied here existed only in Nagasaki, and only six data points are available.

Assuming a yield of 22 KT and a height of burst of 1640 ft for the Nagasaki detonation, as recommended by Lulejian, the distance from the burst of each of the six applicable data points was converted to a dynamic pressure and plotted in Figure 3-4. Each data point corresponds to a percent damage to the walls, as interpreted by the survey teams. It is expected that the order of 50% damage can be used for general comparison with the analytical results of Figure 3-4.

The 10 and 90% confidence bounds on the data for 50% damage to the walls of the building, calculated using the maximum likelihood estimate method suggested by Lulejian, are also shown in Figure 3-4. These confidence bounds are seen to be in general agreement with the TRW calculated 10 to 90% confidence bounds on damage to the rail beams sufficient to drop the crane. However, since the damage definition and the buildings differ from those used in this study, much significance cannot be attached to the comparison without further study of the responses of the Nagasaki buildings.

3.4 COMPARISON WITH PVN SYSTEM

The Physical Vulnerability System (Reference 6) gives ratings of a range of targets in terms of hardness at the reference yield of 20 KT, with a correction factor for other yields. The equivalent Physical Vulnerability Numbers (PVN) for the

industrial target under consideration were computed to provide a comparison with these data. Curves for targets with various sensitivities to yield, so-called K-factors, were calculated from the formulas given in Reference 6, and were matched with Figure 3-4. For the best estimate curve, the closest PVN number is 12Q9. For the curves at 10 and 90% confidence, the corresponding PVN numbers are 8Q9 and 16Q9, respectively, where confidence is defined as the estimated likelihood that parameters having systematic uncertainty combine to bias the results to the extent indicated.

A comparison was also made between the procedures used in this work and the Newmark method (Reference 7). For a yield of 10 KT, the Newmark method gives a dynamic pressure hardness of 2.7 psi, which compares well with the value of 2.9 psi obtained by the method presented in this report for the same parameter values. The small difference is due mainly to the fact that work hardening was included in the present work, but is neglected in the Newmark method.

3.5 ATTACKER'S REQUIREMENTS

The weapon yields and accuracies required for kill probabilities (P_K) of 0.5 and 0.9 are shown in Figures 3-5 and 3-6. These figures are based on the target hardnesses shown in Figure 3-4, and on a Rayleigh-distributed miss distance. The uncertainty bands shown correspond to the effect of the systematic uncertainties on target hardness and damage distance.

For a 10-KT weapon, for example, a CEP of 1000 ft is needed for a 0.9 probability of severely damaging the building (Figure 3-6). This is the best estimate, or 50% confidence value. To obtain 90% confidence that the 0.9 P_K will actually be achieved, a more accurately guided weapon with a CEP of 750 ft is needed. If systematic uncertainties could be reduced, the CEP requirement for a 0.9 probability of kill with 90% confidence may be relaxed.

A reduction in systematic uncertainties has a similar effect on yield requirements. With a CEP of 1000 ft, for example, a 20-KT weapon is required for a P_K of 0.9 with 90% confidence. This figure could be potentially reduced to nearly 10 KT if the uncertainties could be substantially reduced. It should be noted that if the yield is large enough, CEP requirements are easily met.

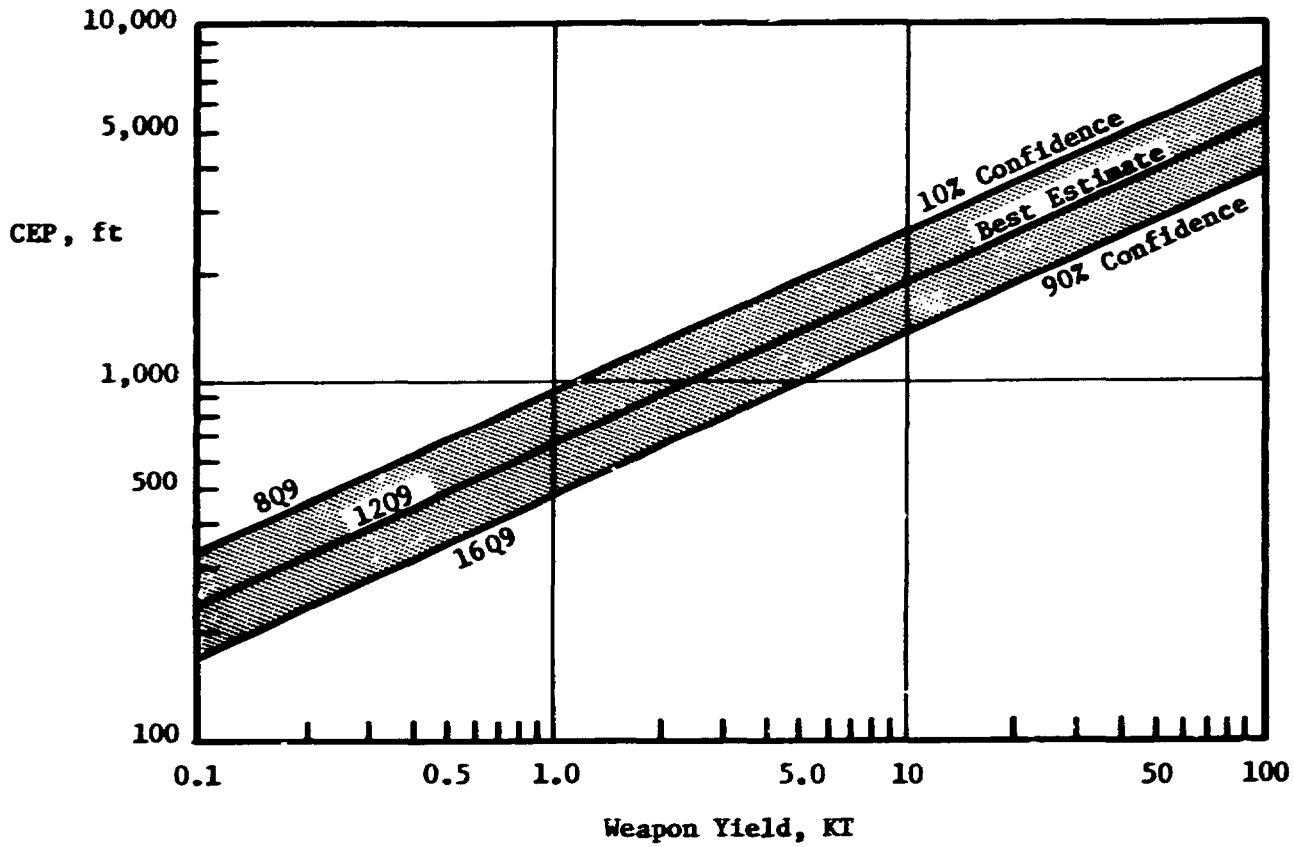

Figure 3-5. Attacker's CEP and Yield Requirements for $P_K = 0.5$

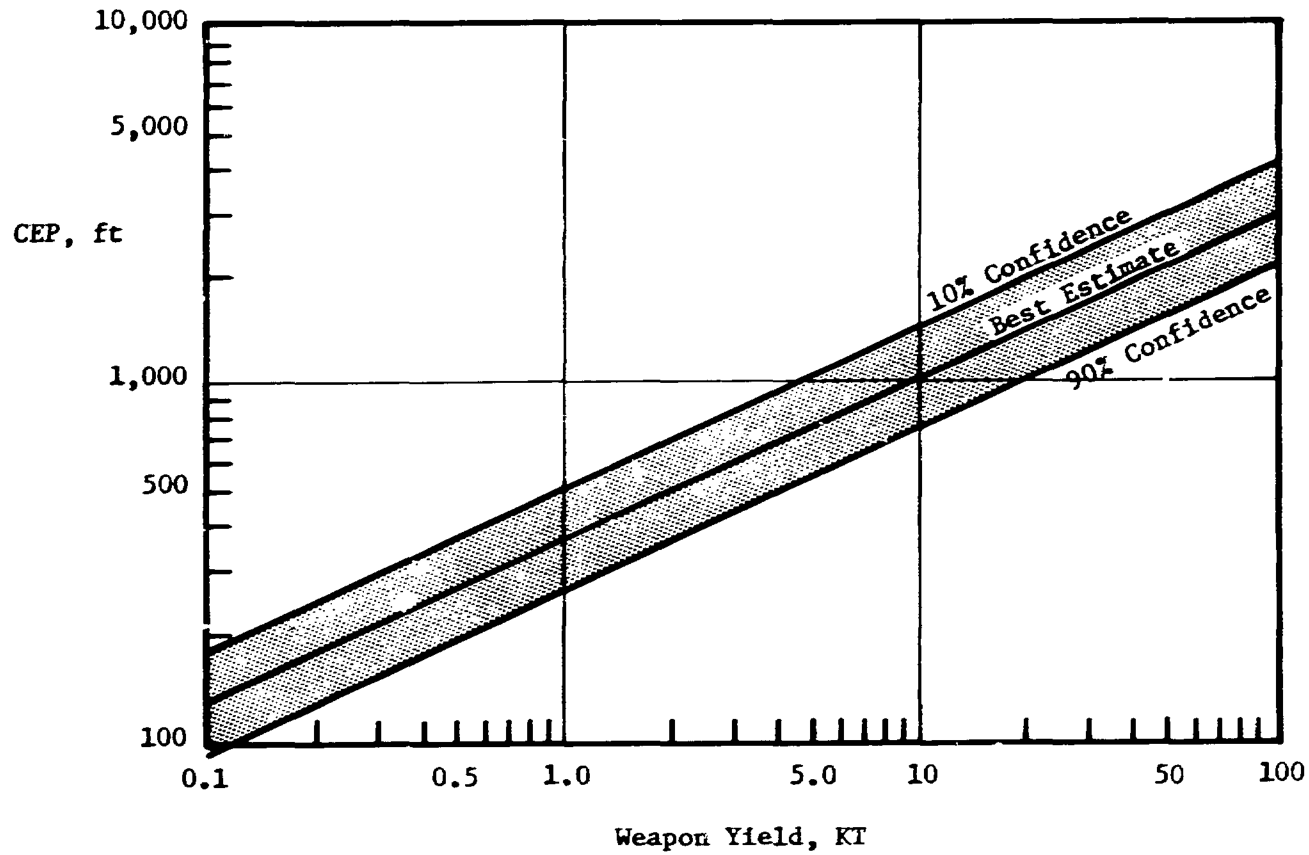

Figure 3-6. Attacker's CEP and Yield Requirements for $k = 0.9$

4.0 BURIED TARGET

Hardened buried structures design/analysis procedures typically consider only a moderate amount of yielding, within the domain of small deformations, and apply simplifying approximations which nearly always add conservatism. This background has generally led to significant underestimation of the overpressure (for a given yield) required to collapse such a structure. In fact, no fully buried concrete structure has collapsed when exposed to nuclear airblast loading; with a number of structures retaining their protective capability at overpressure higher than their predicted collapse load.

For targeting considerations the loading required to damage the structure beyond the point of its subsequent usefulness is of primary interest. In such cases, proper modeling of the large deformation response is of paramount importance and use of conservatisms which have been applied to the design process needs to be reconsidered.

In analyzing the response of a rectangular bunker the typical approach has been to model the roof as a single-degree-of-freedom slab with pinned or fixed supports. When the roof deflection reaches a specified factor (ductility ratio) times an elastic deflection, the structure is considered to have failed. However, the inability of the technical community to predict structural failure loads has led to the identification of several key issues regarding this approach, including (1) Is a single-degree-of-freedom model adequate?, (2) If so, what end conditions should be used?, (3) How is the response affected by loading on the bunker sides?, (4) How does structural damping influence the response?, (5) What is the effect of rigid body motions of the whole bunker?, (6) What is the large deflection force-deformation behavior of the structure?, and finally, (7) What is the failure criterion?

Since the analysis uncertainties have a major impact on the targeting uncertainties, some effort was placed in evaluating the analysis model to use in the study. It was determined, based on comparison with more detailed finite element calculational results, that a single-degree-of-freedom model would be adequate. However, tho model used in this study considered the primary response mode of the complete structure and first-order large deflection force-deformation structural behavior, which includes effects of in-plane stresses. Failure criterion is based on the structure achieving a specified ductility or deflection. Rigid body motions of the bunker have not been included directly in this study. However, a straightforward modification of this analysis is all that is required to incorporate inertial loading effects caused by these motions.

In order to evaluate the elastic response portion of this analysis model the bunker configuration studied is identical to that used in the Reference 8 finite element analysis performed by the Waterways Experiment Station (WES). Since little data are available to properly evaluate the large deformation portion of the response, this study primarily addresses the sensitivity of the response to possible variation in the primary model parameters. Estimates of the uncertainties in the model parameters and in the model itself, along with the sensitivity coefficients, determine the target hardness uncertainty.

4.1 TARGET DESCRIPTION

A box-type reinforced concrete bunker structure is assumed to be sufficiently long so that the response can be considered two dimensional. Obviously, short structures with the same cross section will be stronger. Figure 4-1 shows the 40-ft wide by 25-ft high bunker to be fully buried under 5-ft of overburden. The 5-ft thick roof slab has 2.0% and 1.5% reinforcement at the slab bottom and top, respectively; while the 4-ft thick walls have 1.0% compression and tension steel. Other properties of the bunker structure and surrounding backfill are shown in the figure. The site medium is dry soil over shale with the depth to the soft rock located approximately at the bunker foundation level.

4.2 STRUCTURAL RESPONSE ANALYSIS

The bunker is considered to be subjected to effects caused by the overpressure loading of a nuclear weapon detonation. The side loading on the walls is based on the stress attenuation associated with the overhead airblast loading. Thus, in this analysis, direct-induced and upstream-airblast-induced effects have been neglected. In layered stiffer geologies these effects could be quite significant and the possibility of the wall being more vulnerable than the roof should be considered.

If the primary response mode of the bunker is known, then "simplified" analysis procedures can be applied. These procedures, which assume the bunker to respond only in this primary mode, would be limited by (1) how closely the actual response corresponds to the assumed mode and (2) knowledge of the complete load-deformation relationships. The roof of the bunker considered in this study is expected to be the most critical vulnerability, which is consistent with the assumed response mode. For conditions where the wall response is most critical a different mode would be considered.

During the initial phase of the bunker response the structure behaves elastically, followed by various degrees of plastic deformation and finally collapse. The following subsections address each of the response phases.

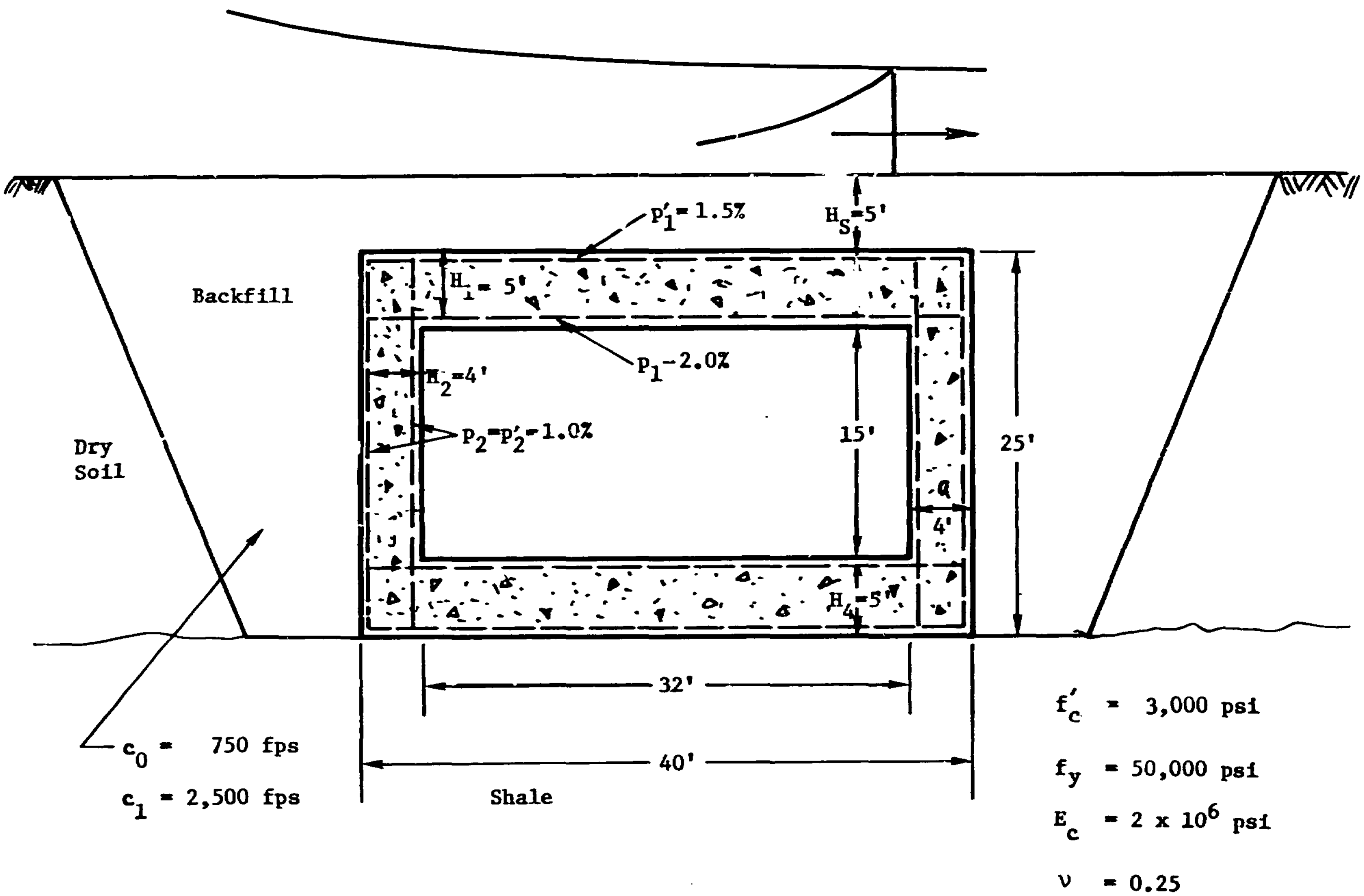

Figure 4-1. Bunker Configuration

4.2.1 Elastic Response Phase

The bunker is modeled as four rigidly connected one-way slabs whose motion are primarily due to bending effects, and therefore, only the midplane motion of these slabs is required to define the complete bunker response. The response of the ith slab is then approximated by (Figure 4-2)

$$y_i = \phi_i(x_i)\ \eta(t) \tag{4-1}$$

where ϕ_i (positive inwards) is the normalized mode shape, η is the single-degree-of-freedom response amplitude and x_i is a coordinate along the midplane of the ith slab (roof, $i = 1$; walls, $i = 2$ and 3; floor, $i = 4$). This results in the undamped equations of motion

$$\rho_i \frac{\partial^2 y_i}{\partial t^2} + D_i \frac{\partial^4 y_i}{\partial x_i^4} = \sigma_i(x_i,t) \tag{4-2}$$

where

$$D_i = \frac{E\ H_i^3}{12(1-\nu^2)} \tag{4-3}$$

and ρ_i, D_i, H_i and σ_i are the mass density per unit midplane area, flexural rigidity, thickness and transverse applied stress, respectively, of the ith slab and E and ν are Young's modulus and Poisson's ratio, respectively, of the concrete. Substituting the Equation (4-1)approximation into the equations of motion, multiplying by ϕ_i, integrating with respect to x_i and summing over the four slabs yields

$$\ddot{\eta} + \omega^2 \eta = \frac{1}{M_{eq}} \sum_{i=1}^{4} \int_0^{L_i} \sigma_i \phi_i dx_i \tag{4-4}$$

where

$$M_{eq} = \sum_{i=1}^{4} \int_0^{L_i} \rho_i \phi_i^2 dx_i \tag{4-5}$$

and

$$\omega^2 = \frac{1}{M_{eq}} \sum_{i=1}^{4} \int_0^{L_i} D_i \frac{\partial^2 \phi_i}{\partial x_i^2}\, dx_i \tag{4-6}$$

are the generalized mass and frequency relationships.

Since this analysis considers a bunker configuration for which the roof vulnerability is most critical, the elastic mode shape (Table 4-1) was based on the deflected shape for a static uniform pressure (w) loading on the bunker roof. The moments M_A and M_B at the intersections between the walls and roof and walls and floor, respectively, are

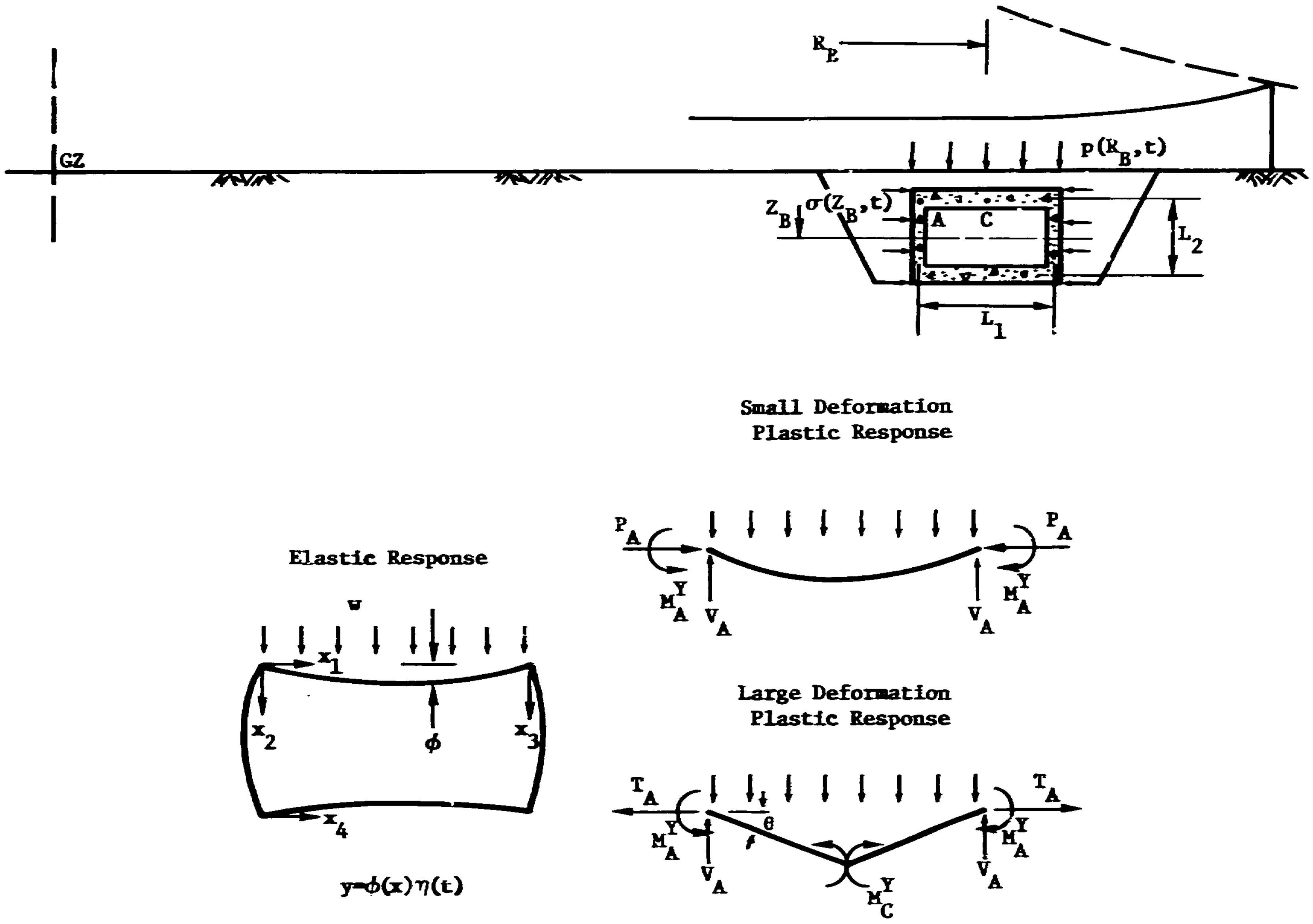

Figure 4-2. Structural Response Analysis

Table 4-1 Bunker Modal Equations

A. Mode Shape

$$\phi_1 = 2\left[\left(\frac{x_1}{L_1}\right) - 2\left(\frac{x_1}{L_1}\right)^3 + \left(\frac{x_1}{L_1}\right)^4\right] + \frac{24M_A}{wL_1^2}\left[-\left(\frac{x_1}{L_1}\right) + \left(\frac{x_1}{L_1}\right)^2\right]$$

$$\phi_2 = \frac{8M_A}{wL_1^2}\;\frac{D_1}{D_2}\;\frac{L_2^2}{L_1^2}\left|-2\left(\frac{x_2}{L_2}\right) + 3\left(\frac{x_2}{L_2}\right)^2 - \left(\frac{x_2}{L_2}\right)^3\right| - \frac{M_B}{M_A}\left|-\left(\frac{x_2}{L_2}\right) + \left(\frac{x_2}{L_2}\right)^3\right]$$

$$\phi_4 = \frac{24M_B}{wL_1^2}\left|-\left(\frac{x_4}{L_4}\right) + \left(\frac{x_4}{L_4}\right)^2\right]$$

where $\dfrac{M_A}{wL_1^2} = \dfrac{1}{12}(1 - k_1)$, $\dfrac{M_B}{wL_1^2} = \dfrac{1}{24} k_1 k_2$

and $k_1 = \dfrac{k_2}{1 - \left(\frac{k_3}{2}\right)^2}$, $k_2 \dfrac{1}{1 + 2\,\dfrac{L_1 D_2}{L_2 D_1}}$, $k_3 = 1 - k_2$

B. Generalized Mass

$$M_{eq} = \frac{\gamma_c}{g}\left\{\left(H_1 + \frac{\gamma_s}{\gamma_c} H_s\right)\left[0.197 - 3.89\,\frac{M_A}{wL_1^2} + 19.2\left(\frac{M_A}{wL_1^2}\right)^2\right] L_1\right.$$

$$\left. + 9.75\;6\;H_2\,\frac{D_1^2 L_2^4}{D_2^2 L_1^4}\left[\left(\frac{M_A}{wL_1^2}\right)^2 - 1.94\,\frac{M_A M_B}{\left(wL_1^2\right)^2} + \left(\frac{M_B}{wL_1^2}\right)^2\right] L_2 + 19.26\;H_1\left(\frac{M_B}{wL_2^2}\right)^2\right] L_1\right\}$$

C. Frequency

$$\omega^2 = \frac{1}{M_{eq}}\;\frac{D_1}{L_1^3}\left\{\left[19.2 - 384\,\frac{M_A}{wL_1^2} + 2304\left(\frac{M_A}{wL_1^2}\right)^2 + 23046\left(\frac{M_B}{wL_1^2}\right)^2\right]\right.$$

$$\left. + 7686\;\frac{D_1 L_2}{D_2 L_1}\left[\left(\frac{M_A}{wL_1^2}\right)^2 - \frac{M_A M_B}{\left(wL_1^2\right)^2} + \left(\frac{M_B}{wL_1^2}\right)^2\right]\right\}$$

determined from conditions of slope continuity at the corners, and the equivalent slab lengths, L_i, are measured from the midpoints of the corners.

In proceeding with the analysis the following simplifying approximations are made regarding the loading: (1) the mass of soil overburden is considered part of the roof which is loaded uniformly by a time varying overpressure, (2) the side loading is also uniform and time varying and is symmetrically applied on both sides of the bunker and (3) the effect of the bottom loading is neglected. Then Equation (4-4) becomes

$$\ddot{\eta} + 2\beta\omega\dot{\eta} + \omega^2\eta = \frac{1}{M_{eq}} \left\{ p(t)\left[\frac{2}{5} - \frac{1}{6} \frac{M_A}{wL_1^2}\right] L_1 \right.$$
$$\left. + 2\, \sigma_2(t) \left[- \frac{2}{wL_1^2} \frac{D_1 L_2^2}{D_2 L_1^2} (M_A - M_B)\, L_2\right]\right\} \qquad (4\text{-}7)$$

where modal damping has been added with β being the percent critical damping and the generalized mass and frequency relationships are given in Table 4-1 (δ being a tracer parameter which is equal to 1.0 for the elastic portions of the response and γ_c and γ_s are the weight densities for concrete and soil overburden, respectively).

Equation (4-7) is directly integrated using the Brode HOB overpressure function (Reference 9) and an expression for lateral load based on the stress attenuation in a bilinear medium (linear loading wavespeed, c_o, and unloading wavespeed, c_1) for a single exponential approximation ($p_o \exp - (t/t_{oo})$) to the surface pressure (Reference 10), viz.,

$$\sigma\,(Z_c,t) = kp_o \left[e^{-\frac{1}{t_{oo}}\left(t - \frac{Z_c}{c_1}\right)} + 2\sum_n \alpha^n\, e^{-\alpha^n \frac{t}{t_{oo}}} \sinh\left(\frac{\alpha^n Z_c}{c_1 t_{oo}}\right)\right] H\left(t - \frac{Z_c}{c_o}\right) \qquad (4\text{-}8)$$

where

$$\alpha = \frac{1-c_o/c_1}{1+c_o/c_1}$$

and p_o is the peak surface overpressure, t_{oo} is the initial slope time intercept, k is the lateral stress coefficient and Z_c is the mid-depth of the structure.

A purely elastic analysis of the baseline bunker configuration was performed to compare results of this simplified analysis with the more detailed WES calculational results. This comparison, which is shown in Figure 4-3, indicates the peak deflection in the WES results to be slightly larger than in the simplified analysis (2.9 in. as compared to 2.7 in.). The waveform comparison is good for the first response cycle; with the WES calculation exhibiting larger equivalent damping at later cycles, as might be expected. In both cases the response oscillates about the quasi-static solution (static deflection

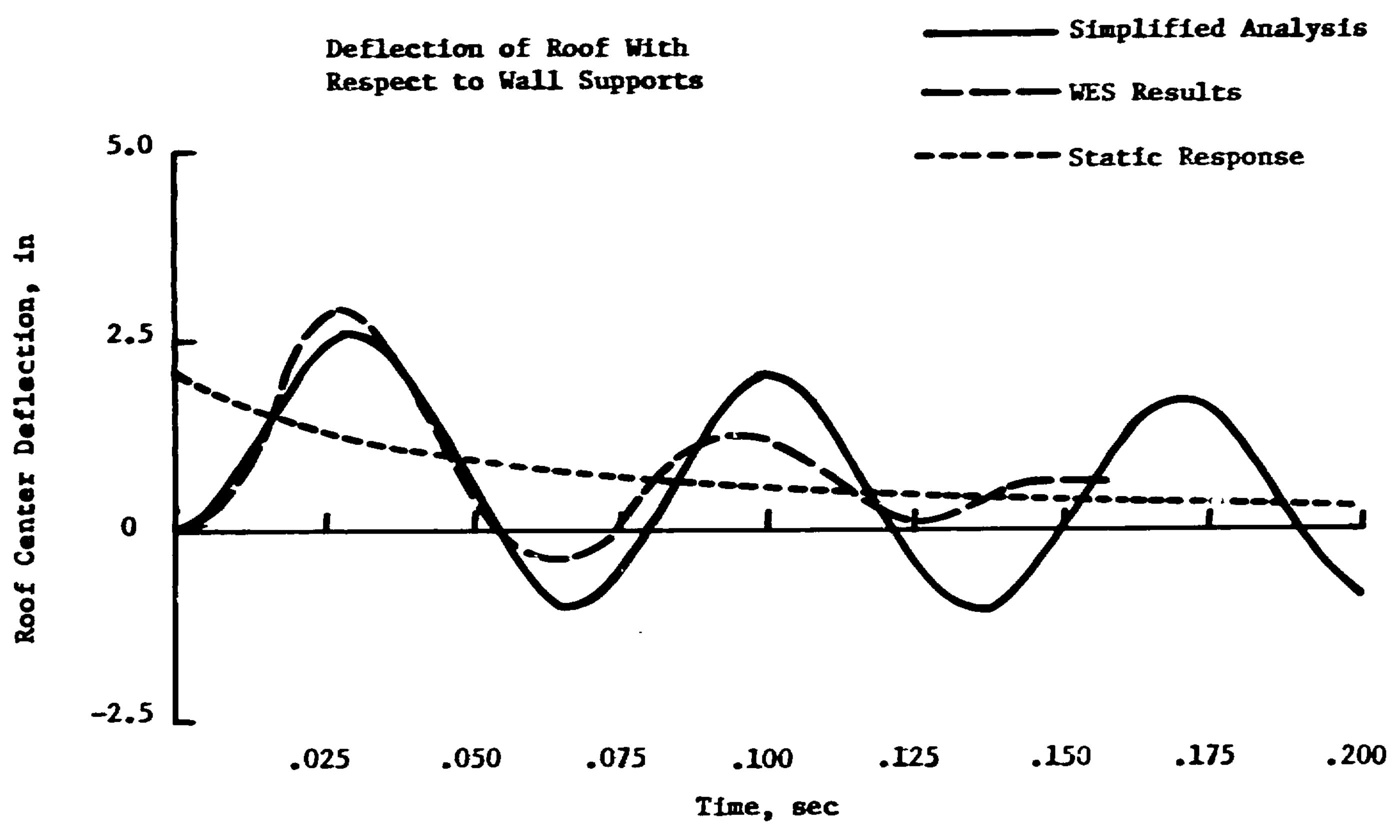

Figure 4-3. Comparison Between WES and Simplified Analysis for Elastic Bunker (300 psi, 1 MT)

caused by the overpressure at a given time).

A comparison between the simplified analysis and WES results for their stiffer backfill case does not show good agreement; probably caused by the approximations used in calculating the side loading (e.g. the side loading does not act until the backfill stress wave gets to the midpoint of the wall). Thus modeling of this loading needs further study. However, the baseline configuration of this study considers the soft backfill whose loading does not have a significant effect on the bunker roof response.

4.2.2 Small Deformation Plastic Response Phase

The elastic analysis is considered to be applicable until the fully plastic moment develops at the top or bottom corners or at the midpoint of the roof. This discussion assumes that the plastic hinge initially develops at the top corners (the case for the baseline bunker configuration), however, similar analysis methodology would be applicable if yielding initiated at the center.

Yielding is governed by the moment-thrust diagram (Reference 11) shown in Figure (4-4). The diagram is a linear fit between (1) the compression capability of the slab with zero moment, P_o, (2) the balance point M_b, P_b, corresponding to the maximum moment, (3) the moment capability in pure bending, M_p and (4) the tension capability of the slab. For compactness the equations governing the points on the yield surface are given in the figure.

It is not known apriori whether yielding at the roof corners will occur within the roof or wall slabs and therefore both possibilities must be checked. The moment is determined from the curvature at the corner as

$$M_A = \frac{4D_1}{L_1^2}(1-k_1)\eta(t) \tag{4-9}$$

while the axial load in the roof, determined from the shear (dM/dx) in the wall just below the corner, is given by

$$P_{A1} = \frac{4D_1}{L_2 L_1^2}\left\{1 - k_1 + \frac{6k_2k_3}{1-k_2 - \frac{k_3^2}{2}}\right\}\eta(t) \tag{4-10}$$

and similarly for the axial loads in the walls

$$P_{A2} = \frac{24D_1}{L_1^3}\eta(t) \tag{4-11}$$

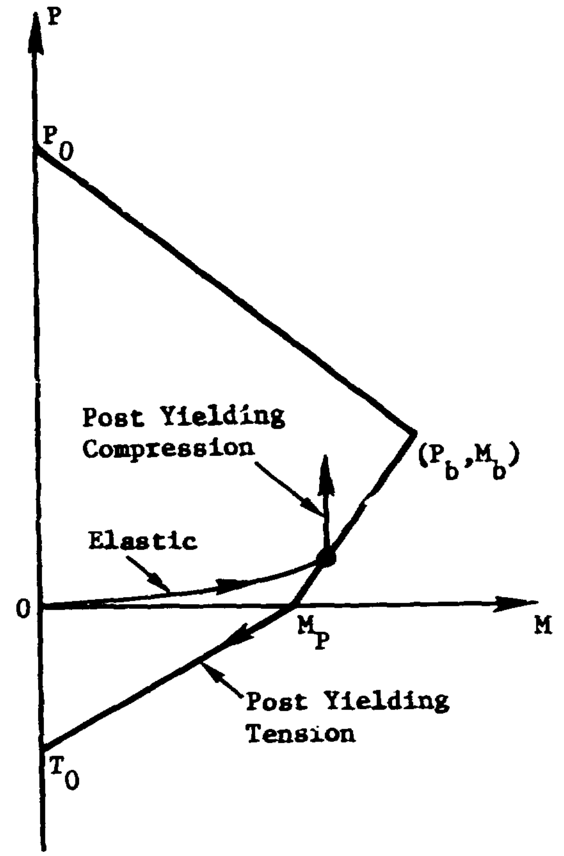

$$P_0 = 0.85\, f'_c\, H_i + f_y (p_i + p'_i) H_i$$

$$T_0 = f_y\, H_i (p_i + p'_i)$$

$$M_p = f_y\, H_i^2 \left[(p_i - p'_i) \left\{ 1 - \frac{0.59 (p_i - p'_i) f_y}{f'_c} \right\} + p'_i \left(1 - \frac{H'_i}{H_i} \right) \right]$$

$$e_b = \left[0.20 + 0.91 \frac{(p_i + p'_i) f_y}{f'_c} \right] H_i$$

$$P_b = f'_c\, H_i \left[\frac{62{,}900 \text{ psi}}{87{,}000 \text{ psi} + f_y} \right]$$

$$M_b = P_b e_b$$

Figure 4-4. Moment-Thrust Yield Criterion

The ultimate moment is reached when M_A, P_{A1} or M_A, P_{A2} reach the yield surface.

When the yield hinge develops the stiffness and primary frequency of the structure decrease and the mode shape must be modified. The load, w, used as a basis for calculating the revised mode shape is taken as the average of the static loads required to (1) develop the yield moment, M_A^Y, at the corners and (2) develop the yield moment, M_C^Y, at the center with M_A^Y applied at the corners. The mode shape is then proportional to the static deflection caused by this load and by the corner moments M_A^Y. Thus, the equation for M_A in Table 4-1 is modified to be

$$\frac{M_A}{wL_1^2} = \frac{1}{\frac{1-k_1}{24} + 4\left(1 + \frac{M_C^Y}{M_A^Y}\right)} \tag{4-12}$$

for purposes of calculating the mode shape ϕ_1, and the corresponding equation of motion is

$$\ddot{\eta} + 2\beta\omega\dot{\eta} + \omega^2\eta = \frac{1}{M_{eq}}\left\{ p(t)\left[\frac{2}{5} - 4\,\frac{M_A}{wL_1^2}\right] L_1 + 2M_A\left[\frac{2}{L_1} - \frac{24M_A}{wL_1^3}\right]\right\} \tag{4-13}$$

where the generalized mass (M_{eq}) and frequency (ω) are as defined in Table 4-1, with the tracer parameter δ equal to zero. Continuity of displacement and velocity at the center of the roof is the basis for determining initial conditions for the plastic region. This small deformation plastic response formulation is considered to be applicable until the fully plastic moment is developed at the center of the roof.

Subsequent response can result in large deformation since three yield hinges have developed. However, resistance to this motion is still provided by the yield moments and by the in-plane tensile forces which develop as the roof deformation becomes large.

4.2.3 Large Deformation Plastic Response Phase

Once three yield hinges develop in the roof then bending effects between hinges will be neglected. The equation of motion of the link between two hinges is given by

$$\ddot{\theta} = \frac{1}{I_A}\left[\frac{1}{8}\,p(t)L_1^2 - M_A^Y - M_C^Y - \frac{TL_1}{2}\,\theta\right] \tag{4-14}$$

with

$$I_A = \frac{1}{24}\,\frac{\gamma_c}{g}\left(H_1 + \frac{\gamma_s}{\gamma_c}\,H_s\right)L_1^3 \tag{4-15}$$

and

$$T = E_S\,(p_1 + p_1')H_1\left[(1 + \theta^2)^{1/2} - 1\right] \qquad (4\text{-}16)$$

is the tension in the roof slab, where E_S is the steel modulus, and θ is the rotation for the link. During this phase of the response the yield moments M_A^Y and M_C^Y are reduced according to the moment - thrust criterion of Figure (4-4). When the maximum tension, T_o, is reached the moments go to zero and the tensile load thereafter is given by

$$T_o = f_y(p_1 + p_1')H_1 \qquad (4\text{-}17)$$

where f_y is the yield stress of the steel.

4.2.4 Structural Capability

Figure (4-5) shows the response of the baseline bunker configuration for a 1-MT/300-psi overpressure loading. Initial yielding occurs at the top of the wall at approximately 0.013 secs. If the subsequent response followed the yield surface of Figure (4-4) the wall moment would continue to increase since the axial load increases, from a state below the balance point. However, whether this additional capability is achievable after yielding occurs is questionable and the yield moment has been taken to be constant when the post-yielding axial compression increases (below the balance point). The yield surface is followed when the axial load decreases, as shown in Figure (4-4).

The moment in the center of the roof continues to increase in the plastic region until the yield criterion for the roof is satisfied. (The initial small moment decrease in this region is an inaccuracy in the model caused by the change in mode shape at the beginning of the first plastic region.) At 0.016 secs three yield hinges have developed in the roof and large deformations can occur which cause tension in the roof slab. The residual roof moment capability associated with this tension is indicated in Figure (4-5). A maximum roof deflection of 8.3 inches occurs at time of 0.084 secs, which corresponds to a ductility of 5.5, with respect to the three yield hinge deflection and a ductility of 8.3 with respect to the elastic deflection.

The bunker response to 10 KT/300 psi and 10 KT/3000 psi overpressure loadings is shown in Figures (4-6) and (4-7), respectively. In the latter case, the large roof tension and correspondingly large shear stresses at the top of the wall would actually tend to be relieved by cantilever yielding at the bottom of the wall (currently not included in the model). However, neglecting this effect would not be expected to have a significant effect on the results since (1) the moment caused by the roof tension was relatively small and (2) the shear loading was not considered to reduce the moment capability at the top of the wall (shown to be constant under large deformation).

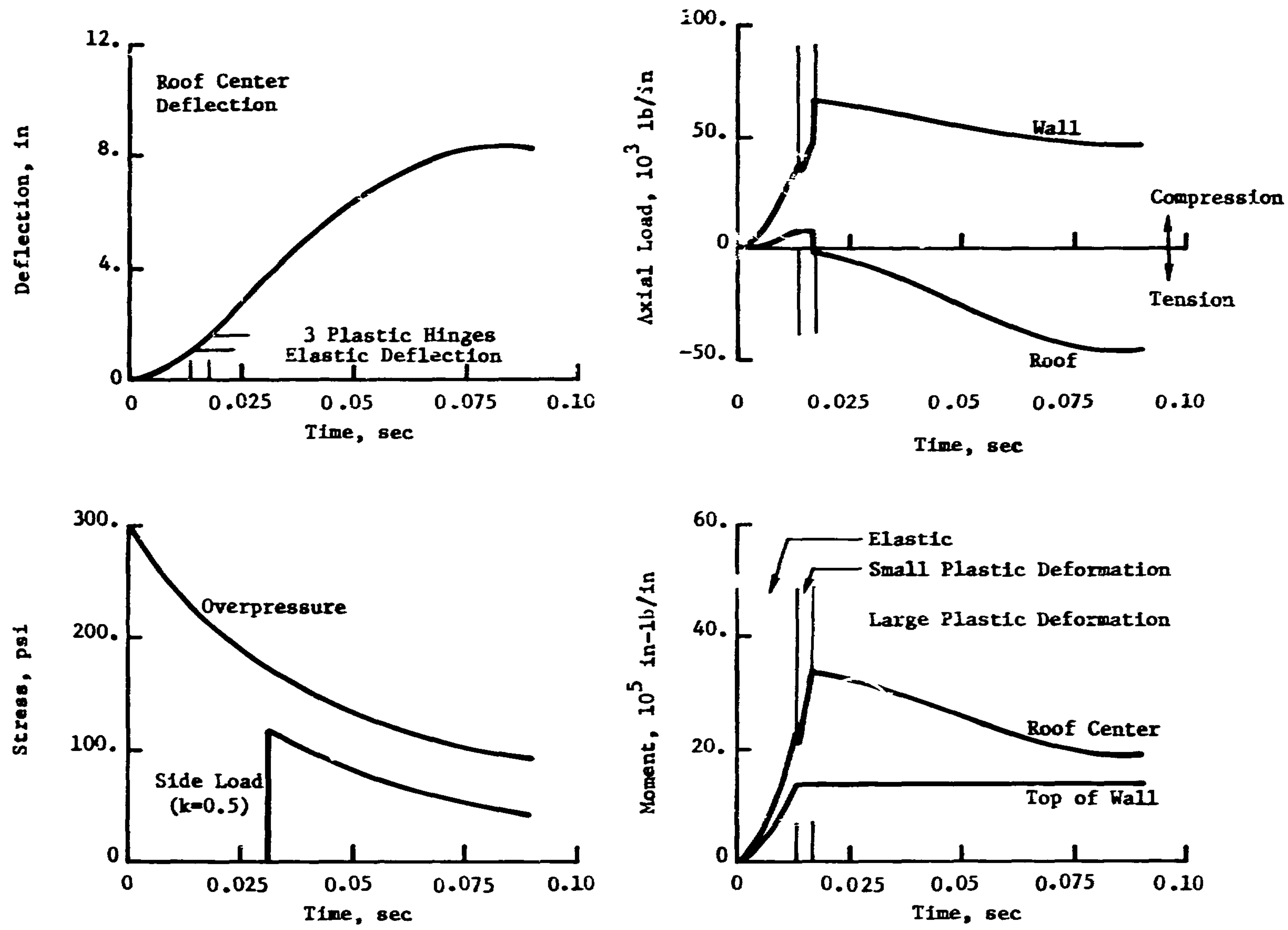

Figure 4-5. Bunker Response for 1 MT, 300 psi Overpressure

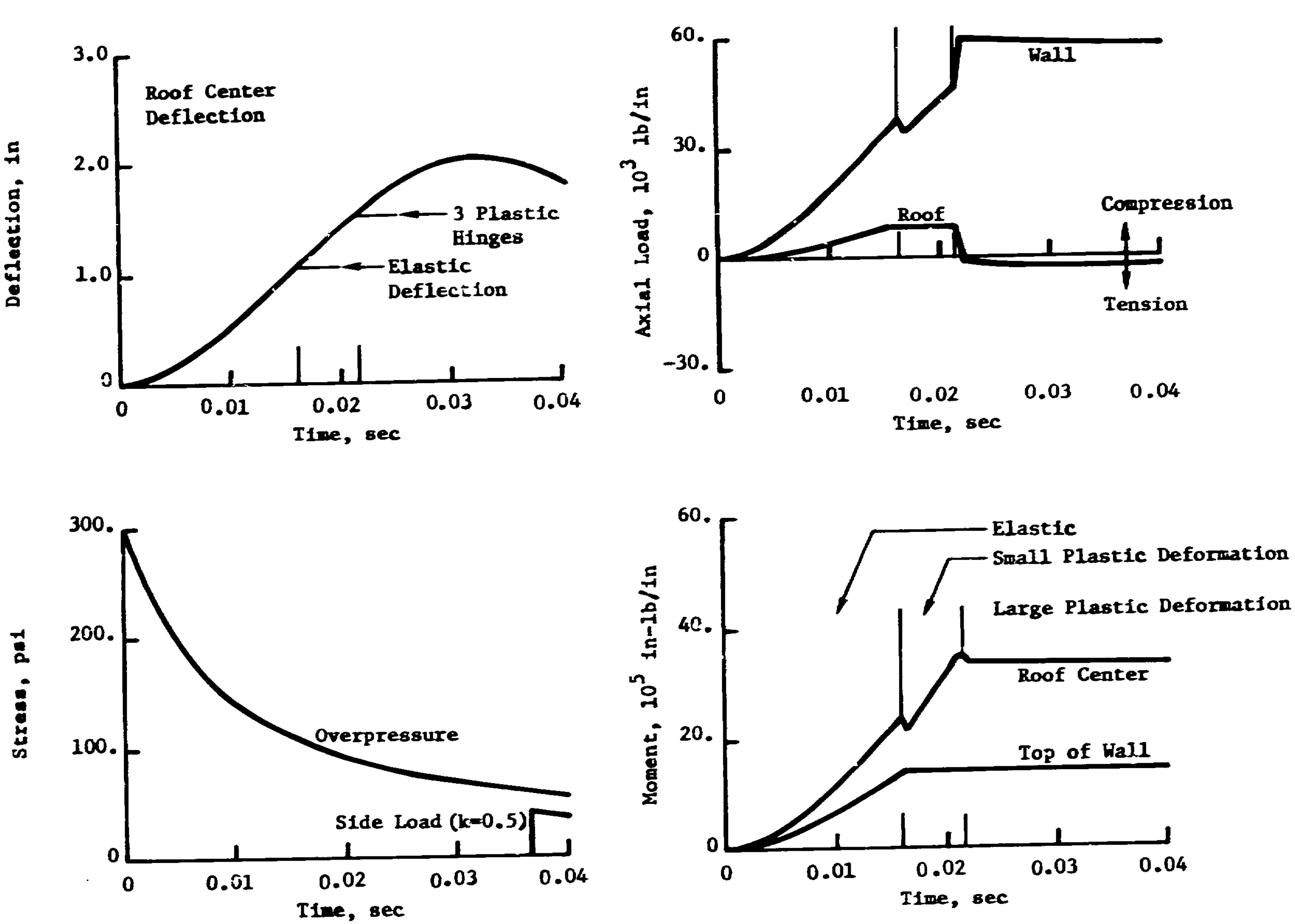

Figure 4-6. Bunker Response for 10 KT, 300 psi Overpressure

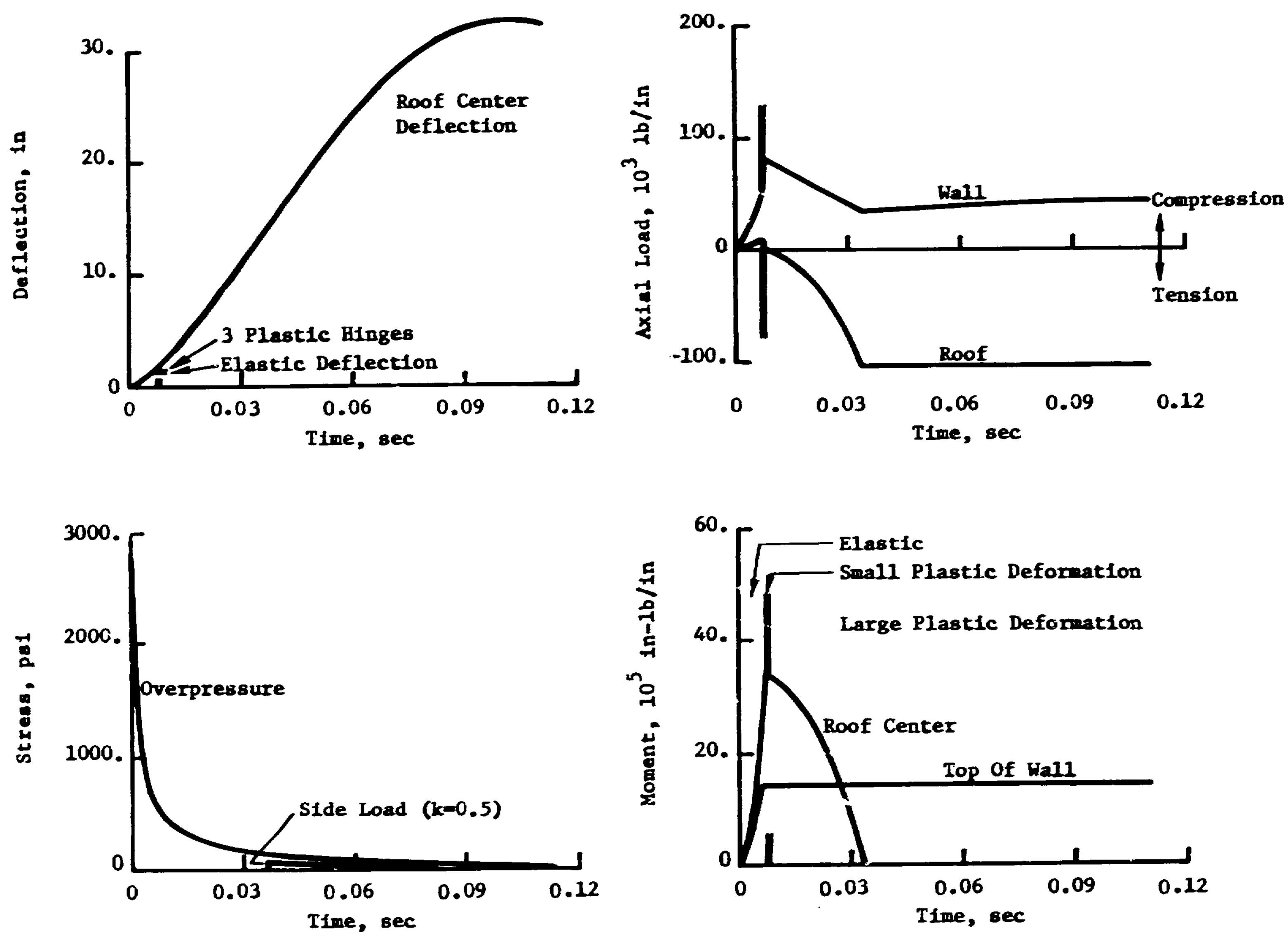

Figure 4-7. Bunker Response for 10 KT, 3000 psi Overpressure

A more general bunker model should include combined large deformation behavior of the roof and walls and yield conditions which include the effects of shear loading in addition to moment and thrust.

Figure (4-8) shows the damage function corresponding to a baseline ductility of 10 (with respect to three yield hinge deformation) and to a center deflection of 10% of the roof span (3.6 ft or $\mu = 28.5$). If the larger deformations were achievable, a significant increase in hardness over the μ of 10 case would result, especially at the lower yields (factor of 2.7 for 10 KT compared with 1.6 for 1 MT). For purposes of further comparison damage functions are shown for a roof slab with simply supported and with fixed end conditions; both for ductilities of 10. The "lower bound" simply supported condition reflects hardnesses lower, by a factor of 1.7 at 10 KT and a factor of 1.5 at 1 MT, than determined from the analysis model used, with the corresponding factors for the "upper bound" fixed end conditions being 1.5 at 10 KT and at 1 MT. To investigate effects of wall yielding reducing the roof tension, additional analysis considered the maximum tension to be zero with the minimum moment equal to the roof capability under pure bending (M_p). These assumptions resulted in a factor of 1.2 increase in hardness for 1 MT and 1.4 increase for 10 KT.

4.3 STRUCTURAL RESPONSE UNCERTAINTIES

Uncertainties in the bunker response are associated with uncertainties in (1) the structure-media interaction (SMI) response analysis, (2) the structure configuration, (3) the material properties and (4) the free field weapon effect environments. Since a generic bunker design has been considered, uncertainty sources associated with intelligence data have not been considered. However, even for a high degree of intelligence data (e.g., structural drawings, material specifications and average engineering site properties are known), uncertainties still exist in such parameters as structural material properties, since contractors typically use materials which have properties better than specification. For example, statistical analysis of two sets of test data for 40,000 psi steel reinforcing bars, summarized in Reference (12), shows the actual strength to be 1.19 and 1.27 times the nominal, respectively. Targeting vulnerability analysis can account for material properties which are better than design specification requirements.

Determination of the bunker hardness uncertainties is based on the methodology in Section 2.2. Sensitivities of the hardness to variation in the analysis parameters are determined as a function of yield from a series of response calculations, for specific yields, each of which consider variation of an individual parameter. Table 4-2 summarizes

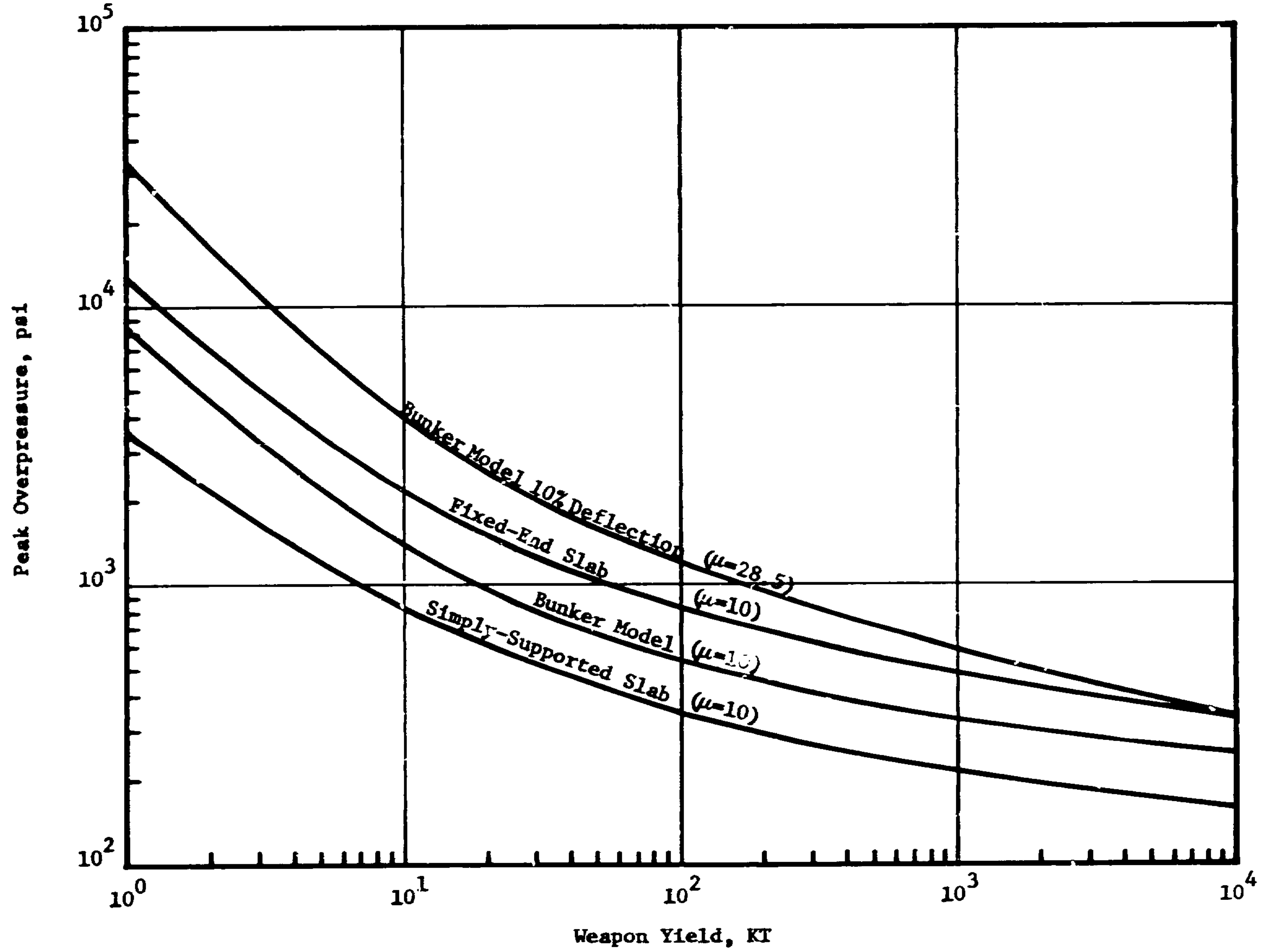

Figure 4-8. Failure Criterion Influence on Target Hardness

Table 4-2 Systematic Bunker Uncertainties

Category	Parameter x_i	Sensitivity $\frac{\partial(\ln p)}{\partial(\ln x_i)}$		2σ x_i Uncert. Factor	2σ Target Hardness Uncertainty	
		10 KT	1 MT		10 KT	1 MT
Structure Media Interaction Response Analysis	Mode Shape, ϕ (1)				1.6	1.5
	Equiv. Roof Span, L_1	2.2	1.9	1.1	1.2	1.2
	Failure Criteria, ϵ	0.90	0.43	1.0	2.7	1.6
	Bending Yield, M_n	0.92	0.64	1.2	1.15	1.12
	Tensile Yield, T_o	0.37	0.16	1.2	1.07	1.03
	Damping, β (2)				1.14	1.05
	Analysis Model				2.0	1.4
	Subtotal				3.7	2.1
Structure Configuration	Steel Area, p & p'	1.45	1.00	1.1	1.15	1.10
	Effective Roof Depth, H_1	2.0	1.8	1.07	1.14	1.13
	Overburden Depth, H_S	0.22	0.11	1.5	1.09	1.04
	Subtotal				1.2	1.1
Material Properties	Steel Yield, f_y	1.34	1.00	1.2	1.3	1.2
	Concrete Modulus, E_c	0.40	0.20	1.2	1.08	1.07
	Backfill Stress Speed, C_o (1)				1.4	1.5
	Subtotal				1.7	1.6
Weapon Effects	Peak Overpressure, p_o	0.73	0.97	1.2	1.14	1.19
	Initial Slope Intercept, t_m	1.52	0.77	1.2	1.32	1.15
	Subtotal				1.4	1.3
		Total			4.0	2.3

(1) $\rho_{ij} = -0.5$

(2) Effect of 20% damping

the key parameter sensitivities for 10 KT and 1 MT yields, the parameter 2σ uncertainty factors and target hardness uncertainty component, corresponding to both yields, associated with each parameter and with the analysis model. The basis for estimating the 2σ uncertainty factors in the analysis parameters is summarized in Table 4-3.

Given reasonably good intelligence information on the structure, it is seen that the analysis parameter uncertainties, particularly the failure criteria, have the most significant effect on target hardness uncertainty. The analysis model uncertainty considers that even if all model parameters are known adequately, the analysis may not predict the response correctly. This uncertainty would be strongly dependent on the bunker being analyzed, i.e., if it were resting on soft soil such that rigid body motions were important or if the side loading had a significant effect on the response, the analysis model uncertainties would be larger than for the bunker considered in this study. Model uncertainties herein are considered to be largest where modeling of the structure yielding is most critical (low yields weapons) but are estimated to be not as large as the effects of failure criteria uncertainties. Additional test data for the large deformation response of model bunkers is required to better define the failure criteria and validate analysis, especially for the low yield weapon loading. Current uncertainties may have an important impact on weapon allocation.

Damping was not considered in the baseline analysis (although it may have been appropriate to consider the order of 20% damping) and it is seen that the effect of damping or its uncertainties is not very significant. The target hardness uncertainties shown in Table 4-2 are based on an analysis which considered 20% damping within the small deformation portion of the response. Rather large hardness increases are obtained if the same damping coefficient is used in both the elastic and plastic region. However, within the plastic region, the damping forces should not imply a total resistance which is significantly beyond the structure capability.

WES analysis results indicate that stiffer backfill media will reduce the roof response. It is estimated that this effect would not be greater than having the roof act as a fixed-end beam. Thus the effect of backfill uncertainty on target hardness is considered to be the same as the effect of mode shape uncertainty. In calculating total target hardness uncertainty this effect is counted only once, which is equivalent to having a correlation coefficient of -0.5 between the target hardness uncertainties corresponding to these parameters. Although used in this study, a lognormal distribution is not an accurate representation of the backfill related uncertainty since softening the backfill does not influence the response nearly as much as stiffening does. However, the approximation will not affect the total uncertainty.

Table 4-3 Basis For Parameter Uncertainty Estimates

Category	Parameter x_i	Uncertainty Factor Basis
Structure Media Interaction Response Analysis	Mode Shape, ϕ	Fixed-end and simply-supported roof beam analysis results
	Equiv. Roof Span, L_1	Width of walls
	Failure Criteria, μ	Difference between $\mu = 10$ and $0.10\ L_1$ roof deflection results
	Bending Yield, M_p	Reference (8)
	Tensile Yield, T_o	Concrete tension capability
	Damping, β	Effect of 20% damping
	Analysis Model	Estimated based on failure criteria related uncertainties
Structure Configuration	Steel Area, p & p'	Engineering estimate
	Effective Roof Depth, H_1	Variation in steel cover
	Overburden Depth, H_S	Design depth of 40 in.; nominal of 60 in.; maximum of 90 in. for the median value
Material Properties	Steel Yield, f_y	Reference (8)
	Concrete Modulus, E_c	Reference (8); $E_c \sim \sqrt{f_c'}$
	Backfill Stress Speed, C_o	Would not have greater effect than fixed-end slab
Weapon Effects	Peak Overpressure, p_o	Reference (9)
	Initial Slope Intercept, t_ω	Same as p_o

The total target hardness uncertainty is considerably larger for 10 KT weapons (2σ factor of 4.0) than for 1 MT weapons (2σ factor of 2.3). This is primarily associated with the fact that at high yield the overpressure required to fail the structure is not nearly as dependent on the ductility as is the case for low yield. On the basis of these results damage function curves corresponding to 10%, 50% (best estimate) and 90% confidence are shown in Figure 4-9. The 50% confidence curve is calculated from the median values of all analysis parameters and, based on related analysis, is only very slightly different from the actual median hardness.

4.4 COMPARISON WITH PVN SYSTEM

For the best estimate curve, the closest PVN (Reference 6) is 37P7. For the 10 and 90% confidence curves, the corresponding numbers are 33P6 and 41P7, respectively.

4.5 ATTACKER'S REQUIREMENTS

Attacker requirements generally consider probabilities of kill, P_K, of much greater than 50%. Random variations will have some influence on these requirements since the targeting may need to consider near-worst-site conditions. However, these are generally negligible compared to the random variations introduced by the CEP distribution.

Table 4-4 gives estimates of random variation effects for both the 10 KT and 1 MT yields. Based on these data and on the systematic uncertainty, the weapon yield and CEP accuracy required for P_K of 0.5 and 0.9 was calculated. The results are shown in Figures 4-10 and 4-11 for confidence levels of 10, 50 and 90%. Table 4-4 gives estimates of random variation effects for both the 10 KT and 1 MT yields. However, as discussed in Section 2, these effects do not significantly influence targeting requirements.

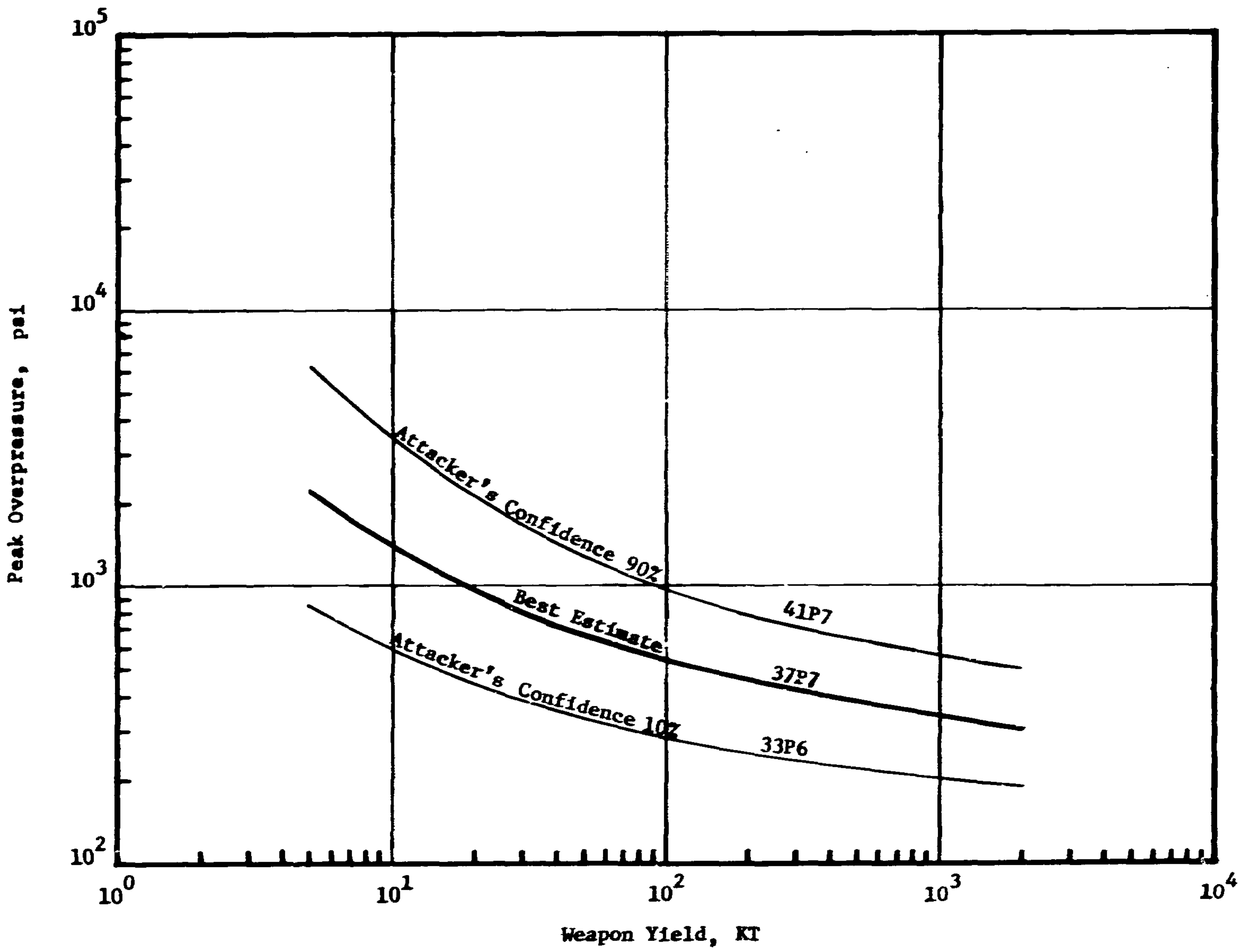

Figure 4-9. Target Hardness

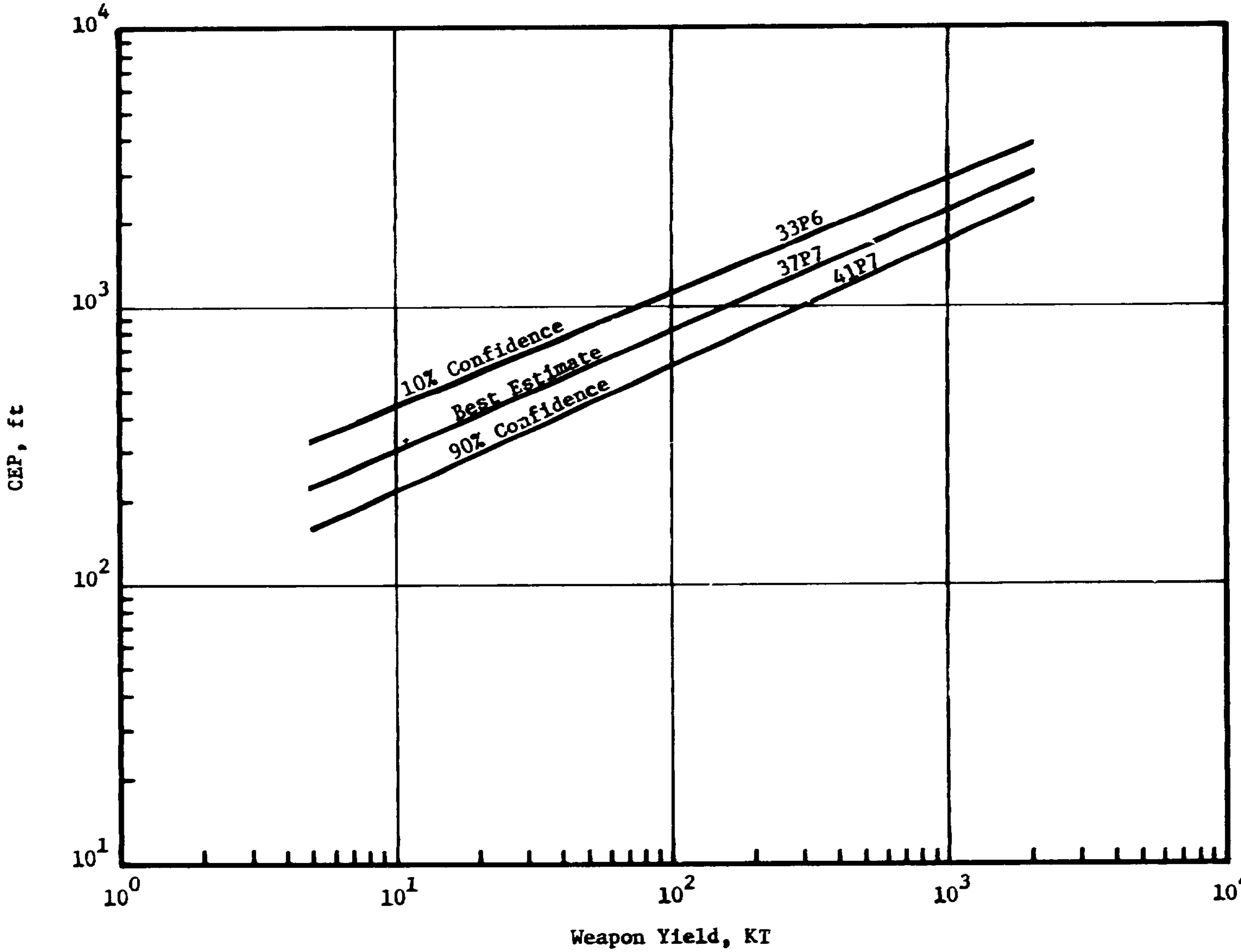

Figure 4-10. Attacker's CEP and Yield Requirement for $P_K = 0.5$

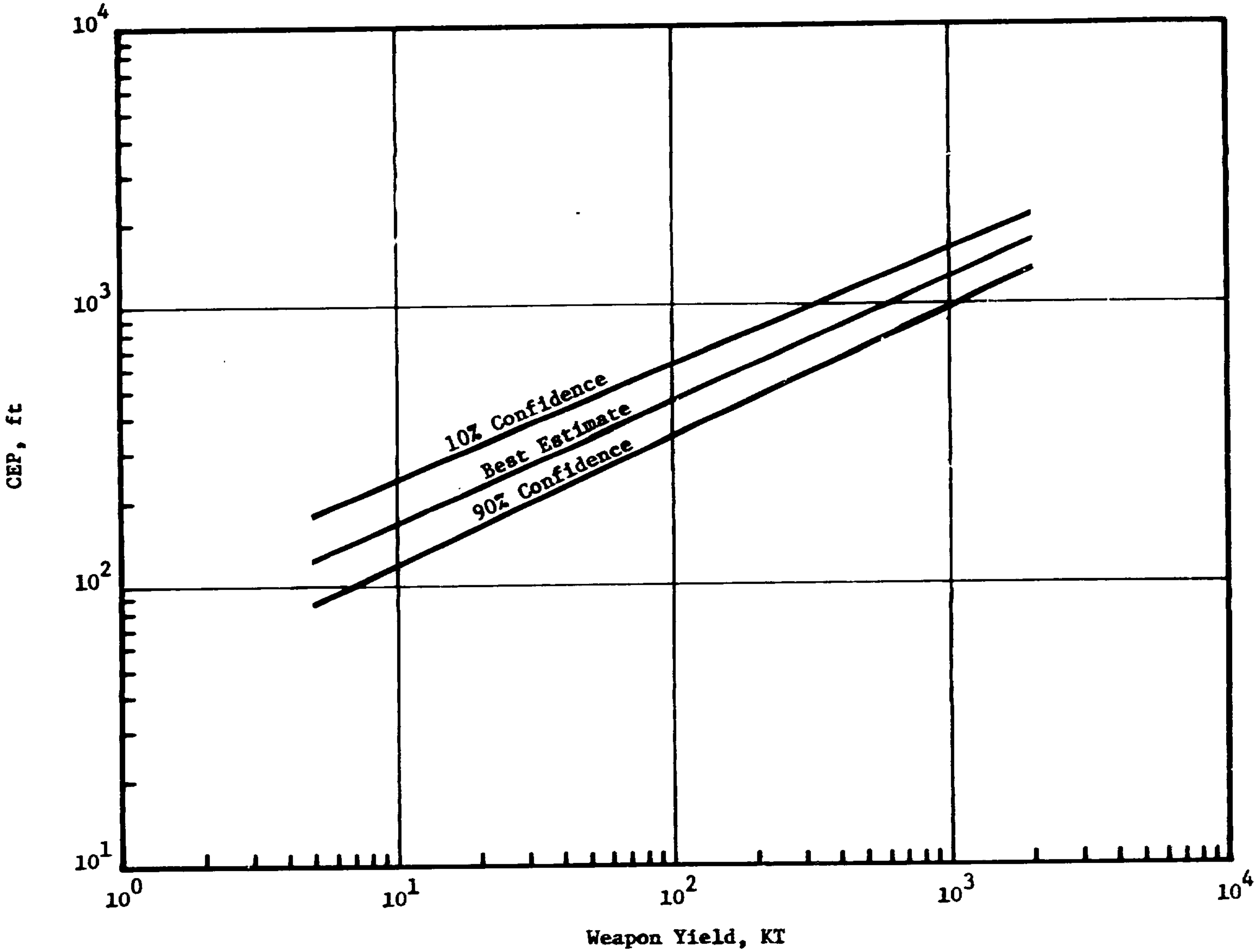

Figure 4-11. Attacker's CEP and Yield Requirement for $P_K = 0.9$

Tatle 4-4 Bunker Random Variations

Category	Parameter x_i	Sensitivity $\frac{\partial(\ln p)}{\partial(\ln x_i)}$		2σ x_i Uncert. Factor	2σ Target Hardness Uncertainty	
		10 KT	1 MT		10 KT	1 MT
Structure Configuration	Steel Area, p and p'	1.45	1.00	1.0	1.0	1.0
	Effective Roof Depth, H_1	2.0	1.8	1.04	1.08	1.07
	Overburden Depth, H_S	0.22	0.11	1.5	1.09	1.04
	Subtotal				1.1	1.1
Material Properties	Steel Yield, f_y	1.34	1.00	1.2	1.3	1.2
	Concrete Modules, E_c	0.40	0.20	1.2	1.08	1.04
	Backfill Stress Speed, C_o				1.6	1.5
	Subtotal				1.7	1.6
Weapon Effects	Peak Overpressure, p_o	0.73	0.97	1.1	1.07	1.10
	Initial Slope Intercept, t_{α}	1.52	0.77	1.1	1.16	1.08
	Subtotal				1.2	1.1
		Total			1.8	1.6

5.0 CONCLUSIONS

This study demonstrates the use of an analytical methodology for the evaluation of the uncertainties associated with the prediction of target vulnerability. Two types of uncertainties are properly distinguished, namely: random variations, which represent actual physical variations; and uncertainties which represent potential bias between the real world and the perceived world of the analytical models and model parameters.

Random variations affect the damage probability of a given target (or the expected number of damaged targets for attacks on similar targets) and are treated adequately by the Physical Vulnerability System. However, the more significant systematic uncertainties are not treated adequately by this system. Where high confidence of high target damage probability is required, the targeting requirements for most cases are governed by the systematic uncertainties.

The targeting uncertainties for the industrial building studied are largely associated with the unique construction of a heavy crane building. These uncertainties could be reduced by experiments designed to provide force-versus-deflection data for structures similar to the 50-T crane building analyzed. However, the cost-to-benefit ratio for such experiments would be prohibitive unless correlations could be established between the representative structures tested and a number of industrial targets.

The targeting uncertainties for the buried bunker analyzed are largely associated with the fact that the analytical procedures have not been validated. The results of this study indicate that simplified analytical models which include the primary response mechanisms, such as the effect of wall flexibility and post-yielding resistance, are adequate. An advantage of a mechanistic model over a finite element analysis is that it is not restricted to a continuum description of the structure analyzed.

Additional test data are needed in several areas to reduce the uncertainties in the present analysis. Dynamic testing should consider representative construction techniques, backfill placement, and site media where possible. Initial testing should consider the smallest size models for which these conditions could be satisfied. The airblast loading should be simulated for times corresponding to structural failure. Both high and low yield testing is desirable, but the high pressure, low yield end of the hardness curve should be emphasized since the uncertainties are largest. Testing at the high yield end provides baseline hardness data.

Both the simplified analysis model and appropriate finite element analysis should be used for pre-test production and post-test evaluation. To support this effort, several features could be added to the simplified model, including (1) improved treatment of the bunker side loading, (2) rigid body motion of the bunker, and (3) effects of soil arching. The specific modeling of the soil-media-interaction phenomenology needs to be verified by comparison with results of finite element analysis and test data.

6.0 RECOMMENDATIONS

Based upon the results of this study, the following general recommendations are made:

1) Error analyses of target hardness estimates should be associated with each analytically derived target hardness estimate so that the potential users of such information can evaluate the associated risks.

2) The σ_D term of the Physical Vulnerability System should not be used to include systematic errors of analyses. The σ_D term very often has little effect upon the probability of damage. Hence including analytical uncertainty understates the risk of significant errors in estimated damage probabilities.

3) Additional testing of scale model bunkers should establish an empirical basis for predicting large deformation and establish failure criteria of this class of structure.

4) Simple analytical formulations for buried bunker response should be validated with test data.

5) Sensitivity analyses should be conducted to provide a data base to support weapon effectiveness evaluation and research planning.

7.0 REFERENCES

1. W. H. Rowan, et al., "Failure Analysis by Statistical Techniques (FAST), Volume I - User's Manual", DNA 3336F-1, TRW Systems Group, Redondo Beach, September 1974.

2. A. H. S. Ang, W. H. Tang, Probability Concepts in Engineering Planning and Design, Volume I-Basic Principles, John Wiley & Sons, Inc., New York, 1975.

3. A. L. Soux, D. C. S. Liu, "Survivability Assessment of Command, Control, and Communications Facilities", TM 166-77, TRW Defense and Space Systems Group, Redondo Beach, September 1977.

4. V. Y. Krasenskiy, "Civil, Industrial and Agricultural Building", JPRS 50529 Joint Publication Research Service, Department of Commerce, Washington D.C., May 1970.

5. R. D. Daniels, G. R. Johnson, "Statistical Analysis of Japanese Structural Damage Data", DNA 4213, Lulejian & Associates, Inc., Torrance, January 1977.

6. G. C. Binninger, P. J. Castleberry, P. M. McGrady, "Mathematical Background and Programming Aids for the Physical Vulnerability System for Nuclear Weapons", DI-550-27-74, Defense Intelligence Agency, Washington D.C., 1 November 1974.

7. N. M. Newmark, "Design of Structures for Dynamic Loads Including the Effects of Vibration and Ground Shock", University of Illinois, Urbana, July 1963.

8. J. E. Windham, J. O. Curtis, "Preliminary Results for First Series of Structure/Backfill Interaction Calculations", U.S. Army Engineer Waterways Experiment Station, Vicksburg, July 1976.

9. H. L. Brode, "Height of Burst Effects at High Overpressures", DASA 2506, The Rand Corporation, Santa Monica, July 1970.

10. L. Seaman, R. V. Whitman, "Stress Propagation in Soils, Final Report - Part IV", DASA 1266-4, Stanford Research Institute, Menlo Park, June 1964.

11. R. E. Crawford, C. J. Higgins, E. H. Bultmann, "The Air Force Manual for Design and Analysis of Hardened Structures", AFWL-TR-74-102, Air Force Weapons Laboratory, Kirtland AFB, Albuquerque, October 1974.

12. J. A. Blume, J. S. Dalal, K. K. Honda, "Statistical Study on the Strength of Structural Materials and Elements", JAB-99-118, John A. Blume and Associates, Engineers, San Francisco, July 1975.

APPENDIX A FREE FIELD EQUATIONS

A.1 Peak Overpressure

Equation (3-3) of Reference 11 expresses the peak overpressure p_{so} in psi in terms of the yield W expressed in MT and radial distance r expressed in kft created by a surface burst by the equation

$$p_{so} = \frac{3300W}{r^3} + \frac{192}{r}\sqrt{\frac{W}{r}} \tag{A1}$$

A.2 Peak Dynamic Pressure

Equation (3-10) of Reference 11 expresses the peak dynamic pressure q_o (psi) in terms of the peak overpressure p_{so} (psi) and ambient pressure p_o (psi) by the equation

$$q_o = \frac{2.5\ p_{so}^{\ 2}}{p_{so} + 7\ p_o} \tag{A2}$$

A.3 Time Variation of Dynamic Pressure

The peak dynamic pressure occurs shortly after the arrival of the blast pressure and subsequently decays approximately exponentially with time. It is assumed here the dynamic pressure q can be expressed by the equation

$$q = q_o\ e^{-\alpha t} \tag{A3}$$

Approximations of the decay parameter α or the time constant

$$\tau = 1/\alpha \tag{A4}$$

are obtained as follows:

Figure 3-21 of Reference 11 shows the variation of dimensionless dynamic pressure q/q_o with dimensionless time t/t_u. The time t_u represents the duration of the positive phase of the dynamic pressure. Figure 3-21 displays the variation of q/q_o for several peak overpressures

PRECEDING PAGE BLANK

p_{so} (or peak dynamic pressures q_o) for a 1 MT yield weapon. Values of t/t_u read from the curves at $q/q_o = 0.1$ are listed in Table A1 in column 3. (The subscript is appended to denote the time when $q/q_o = 0.1$.) The corresponding p_{so} and q_o values for these curves are listed in columns 1 and 2. Values of t_u are shown in column 4 which have been read from Figure 3-19 in Reference 11, corresponding to the value of p_{so}. Setting $q = 0.1\ q_o$ in Equation (A3) and solving for α gives

$$\alpha = \frac{\ln(10)}{t_1} \tag{A5a}$$

or

$$\tau = \frac{t_1}{\ln(10)} \tag{A5b}$$

Values of τ listed in column (5) in Table A1 are obtained from Equation (A5b).

Figure A1 shows the variation of τ with q_o. The data indicate the variation can be approximated by a straight line on a log-log plot. This implies q_o can be approximated by the equation

$$\ln q_o = \ln(A) + B \ln \tau \tag{A6}$$

The straight line approximation in Figure A1 corresponds to $A = 0.25$ and $B = -2.72$, so that (A6) becomes

$$\ln q_o = -1.39 - 2.72 \ln \tau$$

or

$$\tau = e^{-\left(\frac{1.39 + \ln q_o}{2.72}\right)} \tag{A7}$$

Equation (A7) represents the time constant for a 1 MT weapon. The time

Table A1: Dimensionless Time Corresponding to a Fixed Dynamic Pressure Ratio

①	②	③	④	⑤
Overpressure p_{so} (psi)	Dynamic Press. q_o (psi)	t_1/t_u At $q/q_o = 0.1$ Figure 3-21*	t_u (sec) Figure 3-19*	τ (sec) Eq. (A5b)
10	2	0.43	2.5	0.467
20	8	0.31	2.3	0.310
50	40	0.107	2.9	0.135
100	118	0.086	2.8	0.105

constant for a weapon of yield W(MT) is

$$\tau = W^{1/3} e^{-\frac{a_8 + \ell n q_o}{a_9}} , \quad a_8 = 1.39, \; a_9 = 2.72 \qquad \text{(A8)}$$

*See Reference 11

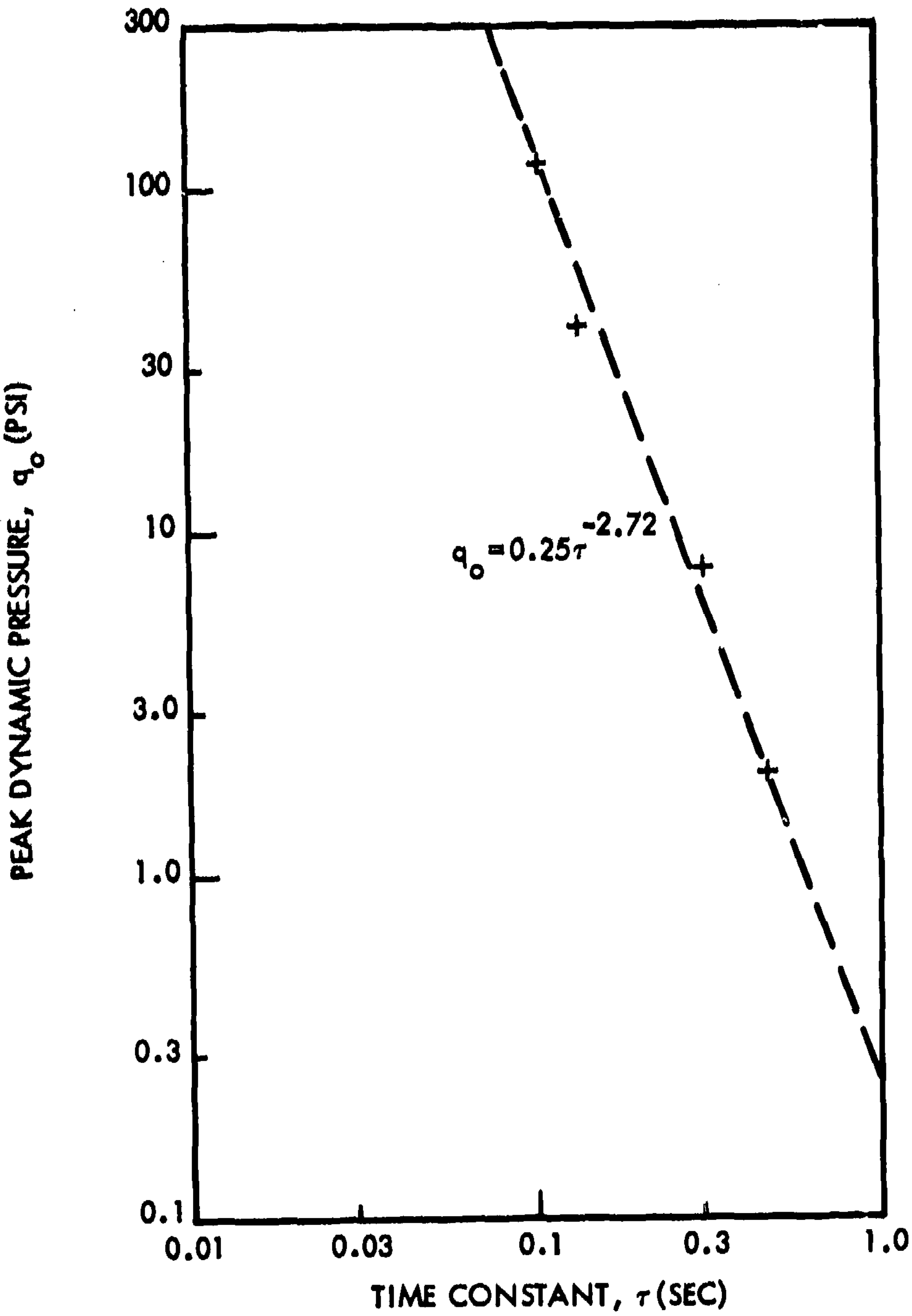

Figure A1: Variation of Time Constant with Peak Overpressure (W = 1MT).

APPENDIX B ELASTO-PLASTIC ANALYSIS MODEL

Solutions of the single-degree-of-freedom elasto-plastic system considered are derived in this section for the idealized system illustrated in Figure B1.

B.1 Elastic Range

The governing differential equation for the first elastic range $0 \leq y \leq y_e$ is

$$\left.\begin{aligned} m\ddot{y} + ky &= P_o e^{-\alpha t} \\ y(0) &= \dot{y}(0) = 0 \end{aligned}\right\} \tag{B1}$$

and the solutions are

$$\left.\begin{aligned} y &= \frac{P_o}{m(\alpha^2 + \omega_1^2)} \left[\frac{\alpha}{\omega_1} \sin\omega_1 t - \cos\omega_1 t + e^{-\alpha t}\right] \\ \dot{y} &= \frac{P_o}{m(\alpha^2 + \omega_1^2)} \left[\alpha\cos\omega_1 t + \omega_1 \sin\omega_1 t - \alpha e^{-\alpha t}\right] \end{aligned}\right\} \tag{B2}$$

where

$$\omega_1 = \sqrt{\frac{k}{m}} \tag{B3}$$

If the disturbance force is not large enough to cause the displacement to exceed the elastic limit y_e, (B2) are valid for all time in which case the displacement increases, reaches a maximum and then decreases. The time at maximum is denoted by t_2 and is obtained by setting $\dot{y}(t_2) = 0$ in (B2) obtaining

$$e^{-\alpha t_2} = \cos\omega_1 t_2 + \frac{\omega_1}{\alpha} \sin\omega_1 t_2 \tag{B4}$$

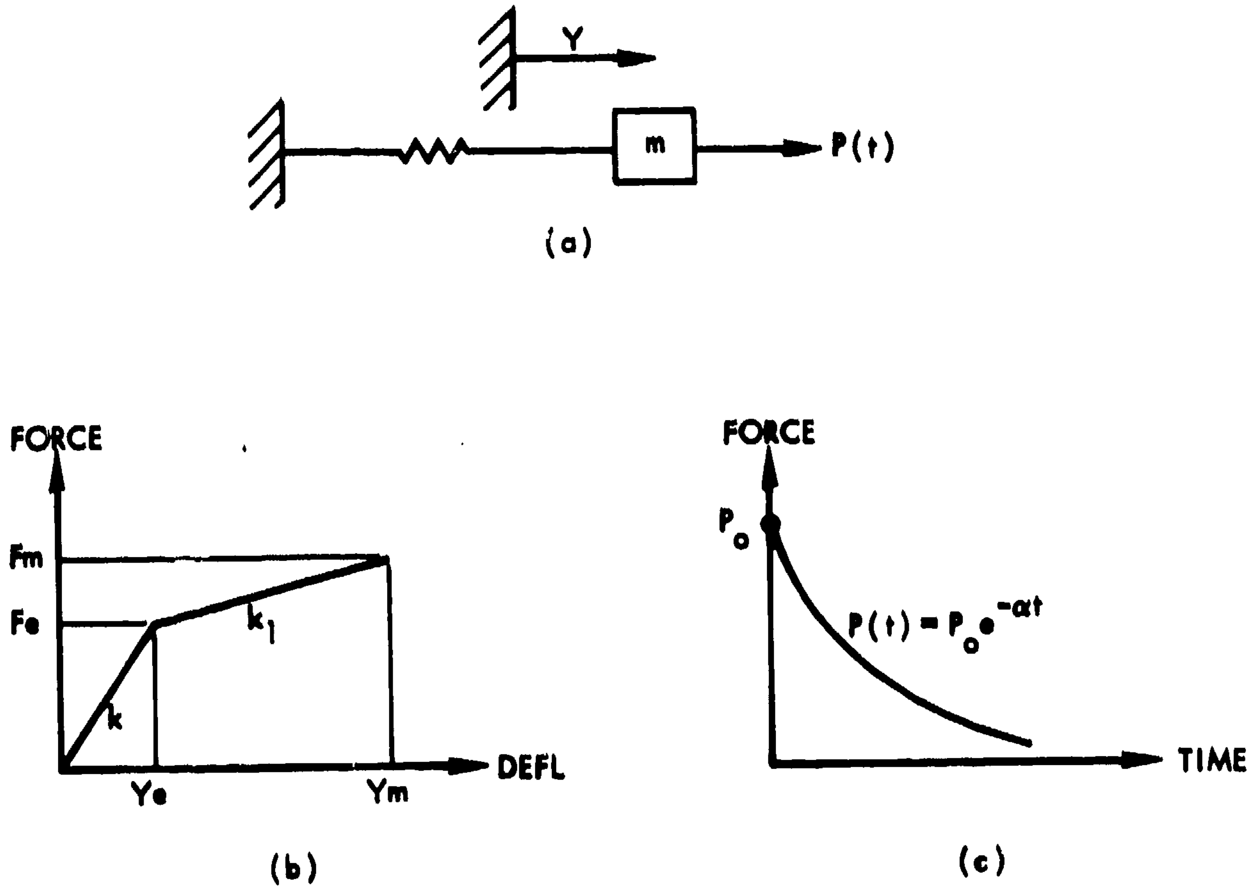

Figure B1: Elasto-Plastic Single-Degree-of-Freedom System (a) System (b) Resistance Force, (c) Disturbance Force.

The corresponding maximum value is obtained from (B2)

$$y_{max} = \frac{P_o}{m(\alpha^2 + \omega_1^2)} \left[\frac{\alpha}{\omega_1} \sin\omega_1 t_2 - \cos\omega_1 t_2 + e^{-\alpha t_2} \right]$$

which can be simplified by making use of (B4) to obtain

$$y_{max} = \frac{P_o}{m\alpha\omega_1} \sin\omega_1 t_2 \tag{B5}$$

Suppose the disturbance force is large enough to cause the displacement to exceed y_e. Then equations (B2) are valid until time t_1 when $y = y_e$. This time is obtained from (B?) by substituting $t = t_1$ and $y = y_e$ to obtain

$$\frac{m(\alpha^2 + \omega_1^2) y_e}{P_o} - e^{-\alpha t_1} = \frac{\alpha}{\omega_1} \sin\omega_1 t_1 - \cos\omega_1 t_1 \tag{B6}$$

The corresponding velocity at time t_1 is

$$v_1 = \dot{y}(t_1) = \frac{P_o}{m(\alpha^2 + \omega_1^2)} \left[\alpha\cos\omega_1 t_1 + \omega_1 \sin\omega_1 t_1 - \alpha e^{-\alpha t_1} \right]$$

This can be simplified by making use of (B6) to eliminate $e^{-\alpha t_1}$ to obtain

$$v_1 = \frac{P_o}{m\omega_1} \sin\omega_1 t_1 - \alpha y_e \tag{B7}$$

B.2 Plastic Range

For those cases where P_o is large enough for the displacement to exceed y_e, the governing equations are $(y > y_e)$

$$m\ddot{y} + k_1 y = P_o e^{-\alpha t} \tag{B8}$$

$$\left.\begin{aligned} y(t_1) &= y_e \\ \dot{y}(t_1) &= v_1 = \frac{P_o}{m\omega_1}\ \sin\omega_1 t_1 - \alpha y_e \end{aligned}\right\} \qquad (B9)$$

The general solution of (B8) is

$$y = A \sin\omega_2 t + B \cos\omega_2 t + \frac{P_o e^{-\alpha t}}{m(\alpha^2 + \omega_2{}^2)} \qquad (B10)$$

where

$$\omega_2 = \sqrt{\frac{k_1}{m}} \qquad (B11)$$

The constants A and B obtained by imposing conditions (B9) are found to be

$$\left.\begin{aligned} A &= C_1 \sin\omega_2 t_1 + \frac{C_2}{\omega_2} \cos\omega_2 t_1 \\ B &= C_1 \cos\omega_2 t_1 - \frac{C_2}{\omega_2} \sin\omega_2 t_1 \end{aligned}\right\} \qquad (B12)$$

where

$$\left.\begin{aligned} C_1 &= y_e - \frac{P_o e^{-\alpha t_1}}{m(\alpha^2 + \omega_2{}^2)} \\ C_2 &= v_1 + \frac{P_o \alpha e^{-\alpha t_1}}{m(\alpha^2 + \omega_2{}^2)} \end{aligned}\right\} \qquad (B13)$$

Let t_3 represent the time when (B10) reaches its maximum value. This occurs when $\dot{y}(t_3) = 0$ which gives

$$\frac{P_o \alpha e^{-\alpha t_3}}{m(\alpha^2 + \omega_2^2)} = A\omega_2 \cos\omega_2 t_3 - B\omega_2 \sin\omega_2 t_3 \tag{B14}$$

The corresponding maximum displacement obtained from (B10) is

$$y_{max} = y(t_3) = A\sin\omega_2 t_3 + B\cos\omega_2 t_3 + \frac{P_o e^{-\alpha t_3}}{m(\alpha^2 + \omega_2^2)}$$

As before, this can be simplified by making use of (B14) to obtain

$$y_{max} = \left(A - B\frac{\omega_2}{\alpha}\right)\sin\omega_2 t_3 + \left(B + A\frac{\omega_2}{\alpha}\right)\cos\omega_2 t_3$$

Upon substituting for A and B and performing a few algebraic steps, one can also express y_{max} as

$$y_{max} = \left(y_e + \frac{v_1}{\alpha}\right)\cos\left[\omega_2(t_3 - t_1)\right]$$

$$+ \frac{1}{\alpha\omega_2}\left(v_1\alpha - \omega_2^2 y_e + \frac{P_o e^{-\alpha t_1}}{m}\right)\sin\left[\omega_2(t_3 - t_1)\right] \tag{B15}$$

APPENDIX C SIDE-ON LOADING ANALYSIS

C.1 Introduction

In this derivation it is assumed the detonation point is located so as to subject the side of the building to the blast wave. The angle between the detonation point and a perpendicular to the rail beams which support the crane is denoted by ψ. When $\psi = 0$, the detonation point is centered on the side of the building and would not subject the front of the building to a dynamic pressure wave. When ψ is different from zero both the side and front of the building are subjected to dynamic pressure loading.

Failure is considered to be initiated when the crane support beam deforms sufficiently to allow the crane to fall to the floor below. The minimum deformation corresponds to the crane located where the maximum rail deformation occurs, nominally at the midpoint of the rail. Failure is considered to be a certainty if the deformations are large enough to exceed the plastic failure limit.

Equations relating weapon yield and range to the two failure limits are derived here for a single degree of freedom representation of the crane rail and its support columns. The single degree of freedom system is considered to be an elasto-plastic system which may have a work hardening behavior after yield begins in the rail beam.

The lateral displacement of the crane rail, denoted by y, corresponds to the total deformation that would be measured at the center of the rail beam. This displacement consists of the sum of the displacement of the top of the vertical columns (where the rail beams are attached) plus the displacement at the center of the rail beam relative to its end attachment points. The single degree of freedom approximation begins with a determination of the linear spring rates and static mode shapes. The spring rate is determined by applying a load P at the center of the crane support beams. One half of this load is reacted by each of the two columns. Equations are derived for various end fixity conditions both at the beam-column interface and also at the

column-ground interface. Once the deformed shapes have been determined, the generalized mass, spring constant and aerodynamic forces are determined. The column-support beam system and its single degree of freedom approximation are illustrated in Figures 1 and B1. Figure C1 shows an idealization of the elastic members when subjected to the load P. A list of the parameters used in this analysis is given in Table C-1.

C.2 Beam Deformed Shape and Spring Constant

The moment at any point x_2 (in the range $0 \leq x_2 \leq (\ell_2/2)$ due to the load P is

$$M = M_o - \frac{P}{2} x_2 \tag{C1}$$

The root moment M_o corresponds to the moment reacted by the column. If the beam is simply supported, the moment M_o is zero. By assuming the beam is uniform one can write

$$EI_2 \frac{d^2 y_2}{dx_2} = M_o - \frac{P}{2} x_2 \tag{C2}$$

and then by assuming

$$y_2(x_2 = 0) = 0 \quad \text{and} \quad \frac{dy_2}{dx_2}\left(x_2 = \frac{\ell_2}{2}\right) = 0 \tag{C3}$$

Equation (C2) integrates to give

$$EI_2 y_2 = \left(\frac{P\ell_2^{\ 2}}{16} - \frac{M_o \ell_2}{2}\right) x_2 + \frac{M_o}{2} x_2^{\ 2} - \frac{Px_2^{\ 3}}{12} \tag{C4}$$

The support moment M_o can be eliminated by introducing a fixity factor F_2 defined as

$$F_2 = \frac{M_o \text{ (corresponding to actual system)}}{M_o \text{ (corresponding to a clamped beam)}} \tag{C5}$$

Table C1 Parameters for Side-on Loading Case

PARAMETER	MEDIAN
neutral axis to outer fibers of beam (in)	6.0
column drag coefficient (dimensionless)	1.3
beam drag coefficient (dimensionless)	1.3
column frontal depth (in)	14.8
beam frontal depth (in)	36
Young's modulus for column (psi)	3×10^7
Young's modulus for beam (psi)	3×10^7
column end fixity factor (dimensionless)	0.5
beam end fixity factor (dimensionless)	0.5
acceleration of gravity (in/sec^2)	386
column area moment of inertia (in^4)	1700
beam area moment of inertia (in^4)	300
column length (ft)	33
beam length (ft)	40
lumped roof mass (lb sec^2/in)	25
ambient pressure (psi)	14.7
range to ground zero (kft)	5
weapon yield (KT)	20
column weight/unit length (lb/ft)	140
beam weight/unit length (lb/ft)	170
minimum displacement of beam for crane drop (in)	6
work hardening parameter (dimensionless)	0.25
column area factor (dimensionless)	2
beam area factor (dimensionless)	2
ductility parameter (dimensionless)	6
beam yield stress (ksi)	36

and the governing differential equation is

$$EI_1 \frac{d^2y_1}{dx_1^2} = \frac{P\ell_1}{2} - \frac{Px_1}{2} \tag{C13}$$

Solutions of (C13) subject to the conditions

$$y_1(x_1 = 0) = 0, \quad \frac{dy_1}{dx_1}(x_1 = 0) = \theta_1 \tag{C14}$$

are

$$\left.\begin{aligned} EI_1y_1 &= (EI_1\theta_1)x_1 + \frac{P\ell_1}{4}x_1^2 - \frac{Px_1^3}{12} \\ EI_1\frac{dy_1}{dx_1} &= EI_1\theta_1 + \frac{P\ell_1}{2}x_1 - \frac{Px_1^2}{4} \end{aligned}\right\} \tag{C15}$$

By letting δ_1 represent the deflection at the top of the column ($x_1 = \ell_1$) (C15) gives

$$\delta_1 = \theta_1\ell_1 + \frac{P\ell_1^3}{6EI_1} \tag{C16}$$

Note that if the base was pinned, the system would be unstable so one cannot introduce a fixity factor based on root moment that can be considered to be zero in the limit. The column fixity factor F_1 is defined as

$$F_1 = 1 - \frac{\delta_1 \text{ (due to rotation of base)}}{\delta_1 \text{ (due to bending of column)}} \tag{C17}$$

With this definition $F_1 = 1$ corresponds to a clamped base, similar to $F_2 = 1$ corresponding to a clamped support for the beam. However, $F_1 = 0$ corresponds to a root support in which the top of the column

With this definition $F_2 = 0$ corresponds to a simply supported beam, and $F_2 = 1$ corresponds to a clamped beam. For a clamped beam

$$M_{oc} = \frac{P\ell_2}{8} \tag{C6}$$

Introducing (C6) into (C5) and solving for M_o gives

$$M_o = F_2\, M_{oc} = \frac{P\ell_2}{8}\, F_2 \tag{C7}$$

which introduced into (C4) gives

$$EI_2 y_2 = \frac{P\ell_2^{\,3}}{16}\,(1 - F_2)\left(\frac{x_2}{\ell_2}\right) + \frac{P\ell_2^{\,3}}{16}\, F_2 \left(\frac{x_2}{\ell_2}\right)^2 - \frac{P\ell_2^{\,3}}{12}\left(\frac{x_2}{\ell_2}\right)^3 \tag{C8}$$

By letting δ_2 represent the deflection at the center (where the load P is applied) relative to the top of the column, (C8) gives

$$\delta_2 = \frac{P\ell_2^{\,3}}{EI_2}\left(\frac{4 - 3F_2}{192}\right) \tag{C9}$$

The corresponding beam spring constant k_b equal to P/δ_2 is

$$k_b = \frac{192\alpha_2}{4 - 3F_2} \tag{C10}$$

where

$$\alpha_2 = \left(\frac{EI}{\ell^3}\right)_{beam} \tag{C11}$$

C.3 <u>Column Deformed Shape and Spring Constant</u>

The moment at any point x_1 of the column shown in Figure C1 due to the end load $P/2$ is

$$M = \frac{P\ell_1}{2} - \frac{Px_1}{2} \tag{C12}$$

has equal displacements contributions due to column bending and column rotation. By making use of (C16) Equation (C17) becomes

$$F_1 = 1 - \frac{\theta_1 \ell_1}{P\ell_1^{\,3}/6EI_1}$$

or

$$\theta_1 \ell_1 = (1 - F_1)\, \frac{P\ell_1^{\,3}}{6EI_1} \tag{C18}$$

which substituted into (C16) gives

$$\delta_1 = (2 - F_1)\, \frac{P\ell_1^{\,3}}{6EI_1} \tag{C19}$$

Hence, the column spring constant $k_c = (P/2)/\delta_1$ becomes

$$k_c = \frac{3\alpha_1}{2 - F_1} \tag{C20}$$

where

$$\alpha_1 = \left(\frac{EI}{\ell^3}\right)_{\text{column}} \tag{C21}$$

By making use of (C19) Equation (C15) gives the deflection at any point to be

$$y_1 = \frac{P}{12\alpha_1} \left[2(1 - F_1)\, \frac{x_1}{\ell_1} + 3\left(\frac{x_1}{\ell_1}\right)^2 - \left(\frac{x_1}{\ell_1}\right)^3 \right] \tag{C22}$$

C.4 Effective Spring Constant

The effective spring constant of the single degree of freedom approximation is composed of a parallel combination of two column

springs in series with the beam spring. Hence, the effective spring constant k is

$$k = \frac{(2k_c)(k_b)}{2k_c + k_b} \tag{C23}$$

where k_c and k_b are given in (C10) and (C20).

C.5 Relation Between Beam Yield Stress and Deformation

The deflection y that produces a bending stress equal to the yield stress in the outermost fibers of the beam is denoted by y_e. The corresponding relative deformation in the beam is denoted by δ_{2e}. The relation between the yield stress σ_y and the deformation of single degree of freedom system y_e is derived in this section. The total deformation of the single degree of freedom system y is related to column and beam deformations by the equation

$$y = \delta_1 + \delta_2 \tag{C24}$$

Since the same force exists in the equivalent system, the beam and in the columns, one can write

$$ky = 2k_c\delta_1 = k_b\delta_2 \tag{C25}$$

From (C23), (C24) and (C25) one obtains the relative deformation of the beam center δ_2 and the deformation of the top of the column δ_1 for a given total deformation y to be

$$\left.\begin{aligned} \delta_1 &= \left(\frac{k}{2k_c}\right)y \\ \delta_2 &= \left(\frac{k}{k_b}\right)y \end{aligned}\right\} \tag{C26}$$

The maximum bending moment occurs at the center of the beam and according

to Equation (C8) is (sign was changed to make moment positive)

$$M_{max} = EI_2 \left. \frac{d^2y_2}{dx_2^2} \right|_{x_2=\ell_2/2} = \frac{P\ell_2}{8} (2 - F_2) \tag{C27}$$

The maximum moment can be expressed in terms of δ_2 by solving (C9) for P and introducing the result in (C27) to obtain

$$M_{max} = \frac{24EI_2\delta_2}{\ell_2^2} \left(\frac{2 - F_2}{4 - 3F_2}\right) \tag{C28}$$

and the corresponding maximum bending stress σ_{max} in the outer fibers located a distance C from the neutral axis is

$$\sigma_{max} = \frac{M_{max}C}{I_2} = \frac{24EC}{\ell_2^2} \left(\frac{2 - F_2}{4 - 3F_2}\right) \delta_2 \tag{C29}$$

At a deflection which produces the yield stress one writes $\delta_2 = \delta_{2e}$ and $\sigma_{max} = \sigma_y$ and (C29) gives

$$\sigma_y = \frac{24EC}{\ell_2^2} \left(\frac{2 - F_2}{4 - 3F_2}\right) \delta_{2e} \tag{C30}$$

By making use of (C26) the deflection y_e can also be expressed as

$$\sigma_y = \frac{24EC}{\ell_2^2} \left(\frac{2 - F_2}{4 - 3F_2}\right) \left(\frac{k}{k_b}\right) y_e \tag{C31}$$

C.6 Generalized Mass

The generalized mass m of the equivalent single degree of freedom system is obtained from the equation

$$my^2 = 2\int_o^{\ell_1} y_1^2 dm_1 + 2\int_o^{\ell_2/2} (y_2 + \delta_1)^2 \, dm_2 \tag{C32}$$

which is based on an energy equivalence criteria. The factor 2 in the first integral accounts for 2 columns, while the factor 2 on the second integral is introduced because the integration extends over one half the beam.

In Equation (C32) y represents the displacement of the equivalent single degree of freedom system, y_1 represents the shape of the deformed column under the end load $P/2$, y_2 represents the deformed shape of the beam under the central load P, and δ_1 represents the displacement of the beam supports. Upon replacing y by the expressions (C24) (and then introducing (C19) and (C9)), and substituting (C8) for y_2 and (C22) for y_1 and finally performing the integrations, the results can be put in the form

$$m = K_1 m_1 + (K_2 + \Delta K_2) m_2 \tag{C33}$$

where

$$\left.\begin{aligned}
K_1 &= \frac{512}{105} \frac{\left[470 - 511F_1 + 140F_1{}^2\right]\left(\frac{\alpha_2}{\alpha_1}\right)^2}{\left[4 - 3F_2 + 32(2 - F_1)\,\frac{\alpha_2}{\alpha_1}\right]^2} \\
K_2 &= \left(\frac{1}{35}\right) \frac{\left[272 - 427F_2 + 168F_2\right]^2}{\left[4 - 3F_2 + 32(2 - F_1)\,\frac{\alpha_2}{\alpha_1}\right]^2} \\
K_2 &= 32\, \frac{(2 - F_1)\left[32(2 - F_1)\,\frac{\alpha_2}{\alpha_1} + 5 - 4F_2\right]\left(\frac{\alpha_2}{\alpha_1}\right)}{\left[4 - 3F_2 + 32(2 - F_1)\,\frac{\alpha_2}{\alpha_1}\right]^2}
\end{aligned}\right\} \tag{C34}$$

C.7 Generalized Force

The generalized force of the equivalent single degree of freedom system is obtained from the relation

$$Py = 2\int_0^{\ell_1} y_1 dP_1 + 2\int_0^{\ell_{2/2}} (y_2 + \delta_1)\, dP_2 \tag{C35}$$

which is based on a work equivalence principle. The differential work terms arriving from the dynamic pressure loading are expressed as

$$dP_1 = q(\eta_1 d_1 C_{D1})\, dx_1 \tag{C36}$$

(C36)

$$dP_2 = q(\eta_2 d_2 C_{D2})\, dx_2$$

where q is the dynamic pressure loading, C_D is the drag coefficient, d represents the width of member exposed to the blast pressure. The η factors are introduced to account for a possible increase in effective frontal area resulting from some effect such as the outer skin of the building wrapping around the member and increasing the area exposed to the air blast. Upon introducing the expressions for y, y_1 and y_2 and performing the integrations, as was done for the generalized mass, the generalized force P becomes

$$P = P_1 + P_2 \tag{C37}$$

where

$$\left.\begin{aligned} P_1 &= \frac{1}{2} q \left\{ \frac{16(\eta_1 d_1)\ell_1 \; C_{D1}(7 - 4F_1)\, \frac{\alpha_2}{\alpha_1}}{32(2 - F_1)\, \frac{\alpha_2}{\alpha_1} + 4 - 3F_2} \right\} \\ P_2 &= \frac{1}{2} q \left\{ \frac{(\eta_2 d_2)\ell_2 \; C_{D2}\left[5 - 4F_2 + 64(2 - F_1)\, \frac{\alpha_2}{\alpha_1}\right]}{32(2 - F_1)\, \frac{\alpha_2}{\alpha_1} + 4 - 3F_2} \right\} \end{aligned}\right\} \tag{C38}$$

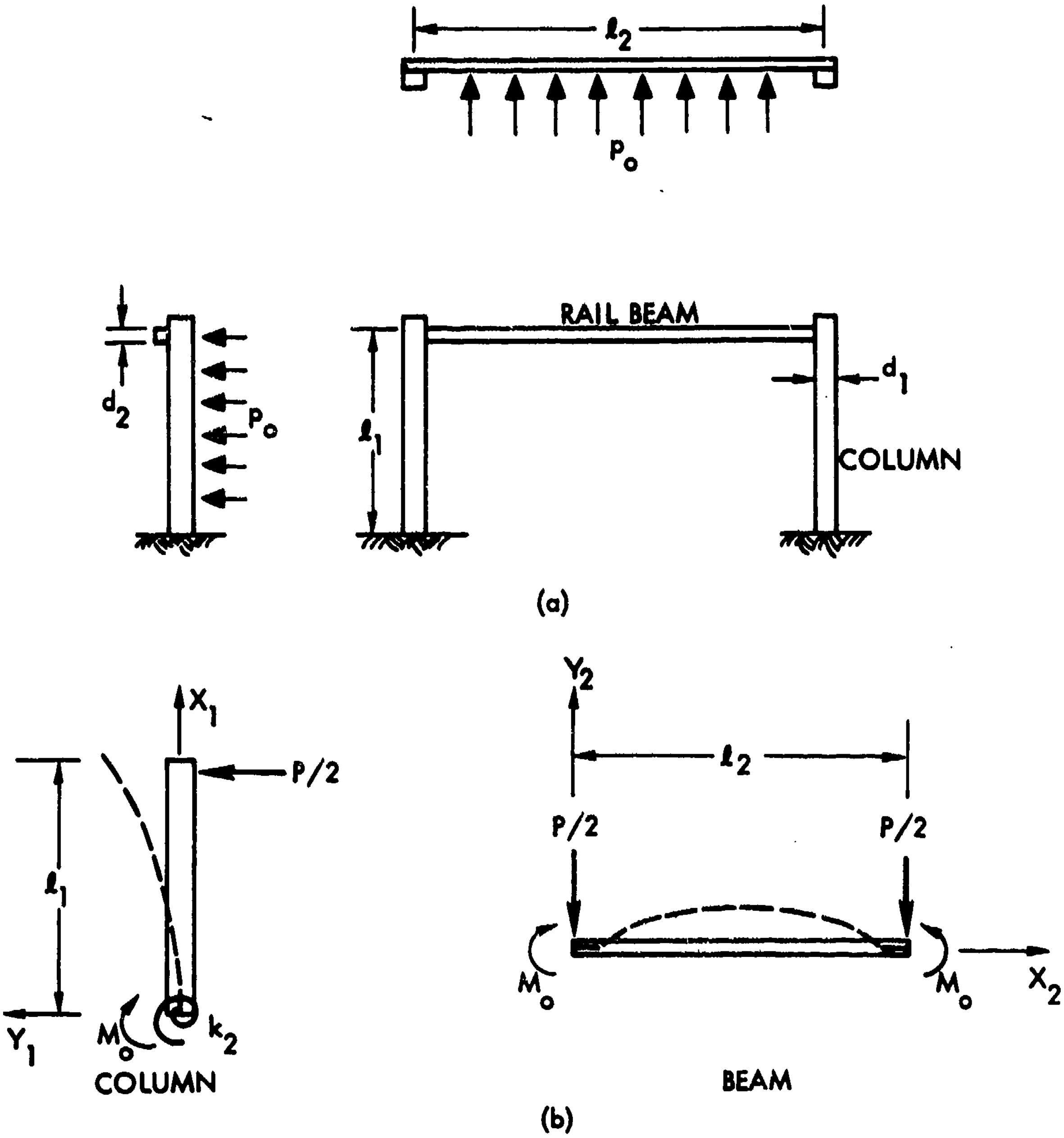

Figure C1: Idealized System Elements.
(a) Elements Subjected to Pressure Loading
(b) Elements Subjected to Centerload P

APPENDIX D. END-ON LOADING ANALYSIS

D.1 Introduction

In this derivation it is assumed the detonation point is located such that it subjects the end of the building to a blast wave pressure loading. The angle between the detonation point and a perpendicular to the crane is denoted by ψ. When $\psi = 0$, the detonation point is directly in front of the end of the building and the blast wave impinges on the end of the building without impinging on the side of the building. When ψ is different from zero a component of the blase wave impinges on the sides of the building.

From Figure D-1, it can be seen that even if $\psi = 0$ and the blast wave subjects the crane to a uniform pressure loading along its length, a yaw moment would exist about the mass center because of an unsymmetrical frontal area exposed to the pressure wave. The rotation produced by the yaw moment is resisted by contact forces between the wheels and rail beam. If the disturbance moment is large enough compared to the resistive moment, the crane will rotate and fail the the floor below. Equations governing this type of failure are derived in this appendix. A list of the parameters used in the derivation are given in Table D-1.

D.2 Single Degree of Freedom Approximation

In general the impinging blast wave produces both a translation and rotation of the crane. Translational motion of even several feet may not necessarily be critical with regard to the crane leaving its track and falling to the floor. On the other hand, only a few degrees of rotation would be sufficient to allow the crane to fall. In this section translational motion is neglected and only the yaw rotational degree of freedom is considered. By letting θ represent the yaw angle, the differential equations governing the motion for the system illustrated in Figure D1 is

$$I_o\ddot{\theta} = M_o - \left[(a - b)\ F_2 + bF_1\right] \mathrm{sgn}\ M_o \qquad \text{(D1)}$$

where I_o is the yaw mass moment of inertia about the mass center and F_1 and F_2 are the rail reaction forces.

PRECEDING PAGE BLANK

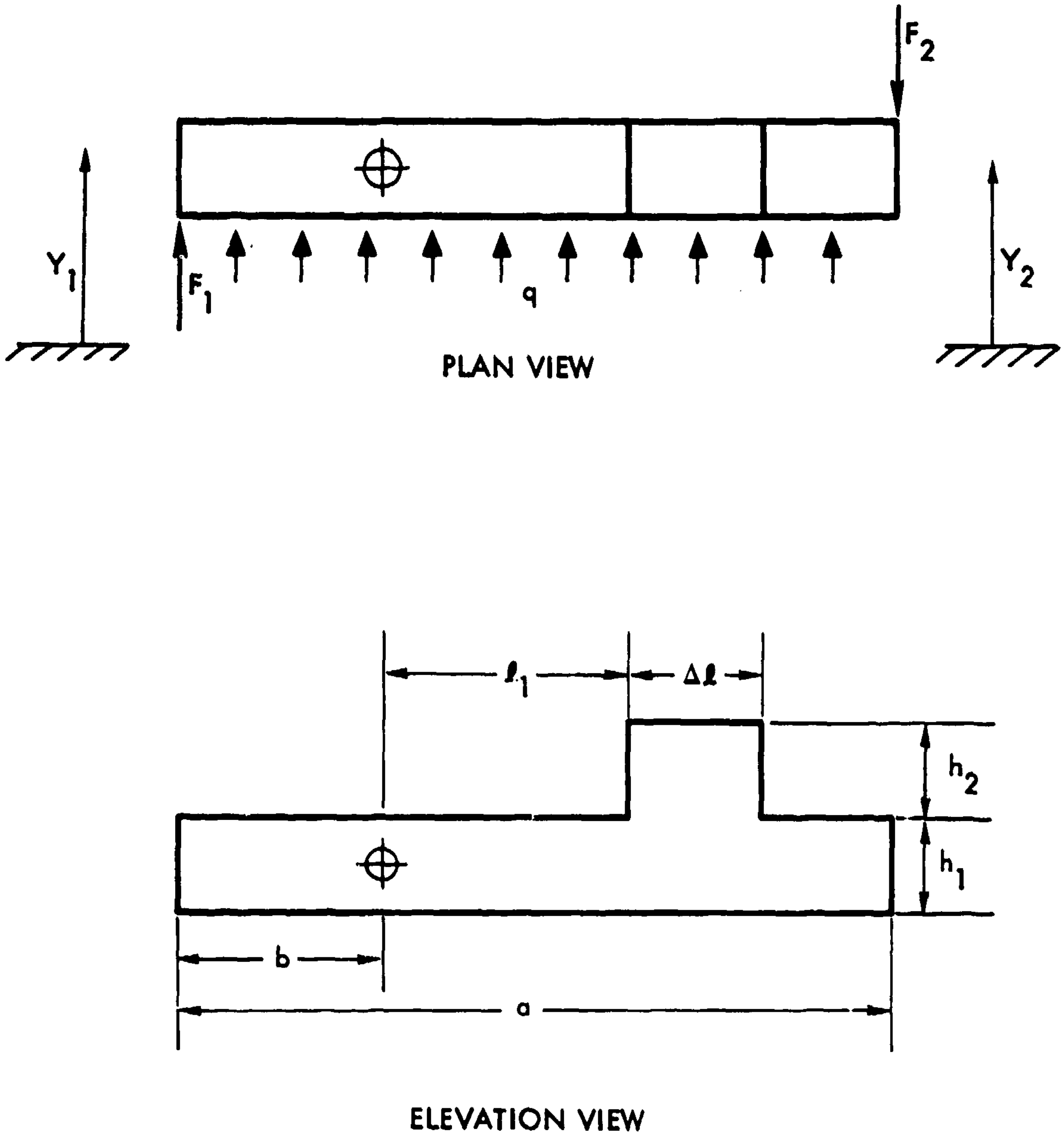

Figure D1: Crane Yaw Motion Model.

Table D-1. Parameters for End-on Loading Case

PARAMETER	MEDIAN
crane length (ft)	78
distance from left rail to crane center of mass (ft)	39
minimum inward motion of crane before failure (ft)	0.5
maximum inward motion of crane before failure (ft)	1.0
drag coefficient (dimensionless)	1.3
frictional resistance at left rail (lb)	1000
frictional resistance at right rail (lb)	1000
moment of inertia about center of mass (ft lb sec^2)	25000
depth of crane (ft)	0.8
depth of operator housing (ft)	2.5
distance from center of mass to housing (ft)	10
length of housing (ft)	4
range to ground zero (kft)	5
crane weight (lb)	2000
weapon yield (KT)	20
area factor (dimensionless)	2

The blast pressure disturbance moment M_o is

$$M_o = q \cos\psi \int_{-b}^{a-b} (\eta h C_D)\, u\, du$$

$$M_o = q_o e^{-\alpha t}\, \eta C_D I_2 \cos\psi \tag{D2}$$

where

$$I_2 = \int_{-b}^{a-b} u\, h\, du = \frac{1}{2} h_1 a(a - 2b) + \frac{1}{2} h_2(\Delta\ell)\left[\Delta\ell + 2\ell_1\right] \tag{D3}$$

In (D2) the change in the normal pressure due to a rotation is neglected because one only needs to consider small changes in θ from its original zero value. Here again the η factor is included to account for a possible increase in effective area upon which the blast pressure acts.

Equation (D1) can be written in the form

$$\ddot{\theta} = Ae^{-\alpha t} - B \tag{D4}$$

where

$$\left.\begin{aligned} A &= \frac{M_o}{I_o} = \frac{q_o \eta C_D \cos\psi}{I_o} \\ B &= \frac{M_R}{I_o} = \frac{(a - b)\ F_2 + bF_1}{I_o} \operatorname{sgn}(M_o) \end{aligned}\right\} \tag{D5}$$

The solution of (D4) for zero initial conditions is

$$\left.\begin{aligned} \dot{\theta} &= \frac{A}{\alpha}\left(1 - e^{-\alpha t}\right) - Bt \\ \theta &= \frac{A}{\alpha^2}\left(\alpha t + e^{-\alpha t} - 1\right) - \frac{1}{2} Bt^2 \end{aligned}\right\} \tag{D6}$$

The time when θ reaches a maximum is denoted by t_1 and is obtained by setting $t = t_1$ and $\dot{\theta} = 0$ in (D6) to obtain

$$\frac{A}{B}\left(1 - e^{-x_1}\right) - x_1 = 0 \tag{D7}$$

where

$$x_1 = \alpha t_1 \tag{D8}$$

One observes that a maximum will only occur when $A > B$, i.e., the disturbance moment must be larger than the resistive moment. When $A > B$ the maximum yaw angle is

$$\theta_{max} = \frac{A}{\alpha^2}\left(\alpha t_1 + e^{-\alpha t_1} - 1\right) - \frac{1}{2} B t_1^2$$

which can be written more simply by making use of (D7) and (D8) to obtain

$$\theta_{max} = \left[\frac{2A - (2 + \alpha t_1)B}{2\alpha^2}\right]\left(\alpha t_1\right) \tag{D9}$$

D.3 Two Degree of Freedom Approximation

The yaw motion θ considered in the preceding section is generalized here to account for crane motion along the rail beams. Let y_1 and y_2 represent the downtrack motion of the left and right ends of the crane. One can describe the crane motion in terms of any two of the three coordinates y_1, y_2 or θ. In this derivation motion is described in terms of y_1 and θ.

The kinetic energy of the system T is

$$T = \frac{1}{2} m\dot{y}_1^2 + \frac{1}{2} I\dot{\theta}^2 + mb\dot{y}_1\dot{\theta}\cos\theta \tag{D10}$$

where I is the yaw mass moment of inertia about the left end. The dynamic pressure force is taken to be

$$q = q_o e^{-\alpha t} \cos(\psi + \theta) \tag{D11}$$

and the track reaction forces are

$$\left. \begin{aligned} F_1 &= f_1 \, \mathrm{sgn}(\dot{y}_1) \\ F_2 &= f_2 \, \mathrm{sgn}(\dot{y}_2) \end{aligned} \right\} \tag{D12}$$

where

$$\left. \begin{aligned} y_2 &= y_1 + a \tan \theta \\ \dot{y}_2 &= \dot{y}_1 + a \, \dot{\theta} \sec^2 \theta \end{aligned} \right\} \tag{D13}$$

The generalized forces associated with the disturbance and reaction forces are

$$\left. \begin{aligned} Q_{y_1} &= -F_1 - F_2 + q \, \eta C_D I_1 \\ Q_\theta &= -F_2 \, a \sec^2 \theta + q \, \eta C_D I_2 \end{aligned} \right\} \tag{D14}$$

where I_2 is given in (D3) and

$$I_1 = \int_0^{\ell} h du = h_1 a + h_2 (\Delta \ell) \tag{D15}$$

By making use of the preceding relations and substituting into Lagrange's equations, one obtains

$$\left. \begin{aligned} m\ddot{y}_1 + (mb\cos\theta)\ddot{\theta} &= G_1 \\ (mb\cos\theta)\ddot{y}_1 + I\ddot{\theta} &= G_2 \end{aligned} \right\} \tag{D16}$$

where

$$\left.\begin{aligned} G_1 &= mb\dot{\theta}^2 \sin\theta - F_1 - F_2 + \eta C_D I_1 q_o e^{-\alpha t} \cos(\psi + \theta) \\ G_2 &= -F_2\, a\sec^2\theta + \eta C_D I_2 q_o e^{-\alpha t} \cos(\psi + \theta) \end{aligned}\right\} \tag{D17}$$

The solution of Equations (D16) for $\ddot{y}_1$ and $\ddot{\theta}$ gives

$$\left.\begin{aligned} \ddot{y}_1 &= \frac{IG_1 - (mb\cos\theta)G_2}{m\left[I - mb^2\cos^2\theta\right]} \\ \ddot{\theta} &= \frac{G_2 - (b\cos\theta)G_1}{I - mb^2\cos^2\theta} \end{aligned}\right\} \tag{D18}$$

Equations (D18) are to be solved subject to the initial conditions

$$y_1(0) = \dot{y}_1(0) = \theta(0) = \dot{\theta}(0) = 0 \tag{D19}$$

DISTRIBUTION LIST

DEPARTMENT OF DEFENSE

Assistant Secretary of Defense
Comm., Cmd., Cont. & Intell.
ATTN: ODASD IA

Assistant to the Secretary of Defense
Atomic Energy
ATTN: Col R. Brodie
ATTN: ATSD (AE)

Defense Advanced Rsch. Proj. Agency
ATTN: STO
ATTN: NMRO
ATTN: TTD, E. Blaise
ATTN: PMO
ATTN: TIO

Defense Civil Preparedness Agency
ATTN: G. Sisson
ATTN: Asst. Director for Research

Defense Communications Agency
ATTN: CCTC/C672
ATTN: Code 930

WWMCCS System Engineering Org.
ATTN: A. Babbitt
ATTN: G. Weathers

Defense Documentation Center
Cameron Station
12 cy ATTN: TC

Defense Intelligence Agency
ATTN: DB-4C2, T. Ross
ATTN: DT-1C
ATTN: DB-4C3
ATTN: DB-4C1
ATTN: RSD-3A
ATTN: DT-2

Defense Nuclear Agency
ATTN: STSP
ATTN: DDST
ATTN: TISI
2 cy ATTN: SPSS
2 cy ATTN: SPAS
3 cy ATTN: TITL

Field Command
Defense Nuclear Agency
ATTN: FCT
ATTN: FCTMOF
ATTN: FCPR

Interservice Nuclear Weapons School
ATTN: Document Control

Joint Strat. Tgt. Planning Staff
ATTN: XPFS
ATTN: DOXT
ATTN: NRI, STINFO Library
ATTN: JLTW-2

DEPARTMENT OF DEFENSE (Continued)

Livermore Division, Fld. Command, DNA
Lawrence Livermore Laboratory
ATTN: FCPRL

NATO School (SHAPE)
ATTN: U.S. Documents Officer

Test Construction Division
Field Command Test Directorate
Defense Nuclear Agency
ATTN: FCTC

Under Secretary of Defense for Rsch. & Engrg.
ATTN: S&SS (OS)

DEPARTMENT OF THE ARMY

BMD Advanced Tech. Ctr.
Huntsville Office
ATTN: CRDABH-S
ATTN: CRDABH-X

BMD Program Office
ATTN: CRDABM-NE

BMD System Command
ATTN: BMDSC-TEN, N. Hurst

Construction Engineering Rsch. Lab.
ATTN: CERL-SL

Dep. Chief of Staff for Rsch., Dev. & Acq.
ATTN: DAMA-AOA-M
ATTN: DAMA(CS), A. Gleim
ATTN: DAMA-CSM-N, G. Ogden

Chief of Engineers
ATTN: DAEN-RDM
ATTN: DAEN-MCE-D

Deputy Chief of Staff for Ops. & Plans
ATTN: Dep. Dir. of Nuclear Chem. Matters
ATTN: MOCA-ADL

Engineer Studies Center
ATTN: DAEN-FES, LTC Hatch

ERADCOM Technical Support Directorate
ATTN: E. Hunter

Harry Diamond Laboratories
ATTN: DELHD-NP
ATTN: DELHD-TI

Redstone Scientific Information Ctr.
U.S. Army R & D Command
ATTN: Chief, Documents

U.S. Army Armament Material Readiness Command
ATTN: MA, Library

PRECEDING PAGE BLANK

DEPARTMENT OF THE ARMY (Continued)

U.S. Army Ballistic Research Labs.
ATTN: A. Ricchiazzi
ATTN: DRXBR-X, J. Meszaros
ATTN: DRDAR-BLE, W. Taylor
ATTN: C. Kingery
ATTN: DRDAR-BLE, J. Keefer
2 cy ATTN: Technical Library

U.S. Army Comb. Arms Combat Dev. Acty.
ATTN: G. Steger
ATTN: LTC Pullen

U.S. Army Communications Cmd.
ATTN: Technical Reference Div.

U.S. Army Engineer Center
ATTN: ATSEN-SY-L

Division Engineer
U.S. Army Engineer Div., Huntsville
ATTN: HNDED-SR

Division Engineer
U.S. Army Engineer Div., Ohio River
ATTN: ORDAS-L

U.S. Army Engineer School
ATTN: ATSE-TEA-AD
ATTN: ATSE-CTD-CS

U.S. Army Engr. Waterways Exper. Sta.
ATTN: J. Ballard
ATTN: G. Jackson
ATTN: W. Flathau
ATTN: J. Strange
ATTN: L. Ingram
ATTN: Library
ATTN: F. Brown

U.S. Army Foreign Science & Tech. Ctr.
ATTN: Research & Concepts Branch
ATTN: Rsch. & Data Branch

U.S. Army Mat. & Mechanics Rsch. Ctr.
ATTN: J. Mescall
ATTN: R. Shea
ATTN: Library

U.S. Army Materiel Dev. & Readiness Cmd.
ATTN: DRCDE-D, L. Flynn
ATTN: DRXAM-TL

U.S. Army Missile R&D Command
ATTN: DRDMI-XS

U.S. ARMY Mobility Equip R&D Ctr.
ATTN: A. Tolbert
ATTN: DRDME-WC

U.S. Army Nuclear & Chemical Agency
ATTN: Library

U.S. Army Training and Doctrine Comd.
ATTN: LTC J. Foss
ATTN: LTC Auveduti

U.S. Army War College
ATTN: Library

DEPARTMENT OF THE ARMY (Continued)

U.S. Military Academy
ATTN: R. La Frenz

U.S. Army Mat. Cmd. Proj. Mngr. for Nuc. Munitions
ATTN: DRCPM-NUC

DEPARTMENT OF THE NAVY

Office of the Chief of Naval Operations
ATTN: Code 604C3
ATTN: OP 03EG
ATTN: OP 981
ATTN: OP 098T8
3 cy ATTN: OP 982

Office of Naval Research
ATTN: ONR 464, T. Quinn
ATTN: ONR 463, J. Heacock
ATTN: ONR 461, J. Warner
ATTN: ONR 715
ATTN: ONR 474, N. Perrone

Civil Engineering Laboratory
Naval Construction Battalion Center
ATTN: W. Shaw
ATTN: Code L08A
ATTN: R. Odello
ATTN: S. Takahashi

Commandant of the Marine Corps.
ATTN: POM

David W. Taylor Naval Ship R & D Ctr.
ATTN: Code 1700, W. Murray
ATTN: Code 160, R. Short
ATTN: Code 2740, Y. Wang
ATTN: Code L42-3
ATTN: Code 177, E. Palmer
ATTN: Code 1740-5, B. Whang

Development Center
Fire Support Branch, MCDEC
ATTN: CAPT Hartineady
ATTN: LTC Gapenski

Naval Air Systems Command
ATTN: F. Marquardt

Naval Electronic Systems Command
ATTN: PME 117-21A

Naval Electronics Systems Command
Southwest Division
ATTN: Commander

Naval Explosive Ord. Disposal Fac.
ATTN: Code 504, J. Petrousky

Naval Facilities Engineering Command
ATTN: Code 03A
ATTN: Code 04B
ATTN: Code 09M22C

Naval Ocean Systems Center
ATTN: E. Cooper
ATTN: Code 4471

Naval Postgraduate School
ATTN: Code 1424
ATTN: Code 2124

DEPARTMENT OF THE NAVY (Continued)

Naval Research Laboratory
ATTN: Shock & Vib. Info. Ctr., H. Pusey
ATTN: Code 2627
ATTN: Code 8403, R. Belsham
ATTN: Code 8440, F. Rosenthal
ATTN: Code 8440, G. O'Hara

Naval Sea Systems Command
ATTN: SEA-9931G
ATTN: Code 03511
ATTN: Code 0351
ATTN: ORD-033
ATTN: ORD-91313
ATTN: SEA-9931, R. Lane

Naval Ship Engineering Center
ATTN: Code 6105
ATTN: Code 09G3

Naval Surface Weapons Center
ATTN: Code F30
ATTN: Code 240, C. Aronson
ATTN: Code E21, G. Matteson
ATTN: Code 240
ATTN: Code U401, W. Kleinerman
ATTN: Code 241
ATTN: Code 243

Naval Surface Weapons Center
Dahlgren Laboratory
ATTN: W. Wishard
ATTN: Technical Library & Information Services Branch

Naval War College
ATTN: Code E11

Naval Weapons Center
ATTN: Code 533
ATTN: C. Austin
ATTN: J. Bowen

Naval Weapons Evaluation Facility
ATTN: Code 10
ATTN: R. Hughes

Strategic Systems Project Office
ATTN: NSP-43
ATTN: NSP-272
ATTN: NSP-273

DEPARTMENT OF THE AIR FORCE

ADCOM/DC
ATTN: KRX

ADCOM/XPD
ATTN: XPX
ATTN: XPDQQ
ATTN: XP

AF Armament Laboratory, AFSC
ATTN: DLYV, J. Collins

AF Geophysics Laboratory, AFSC
ATTN: SUOL, Rsch. Lib.
ATTN: LWW, K. Thompson

DEPARTMENT OF THE AIR FORCE (Continued)

AF Institute of Technology, AU
ATTN: Commander
ATTN: Library

AF Office of Scientific Research
ATTN: NA, Dr. Wolfson

AF Weapons Laboratory, AFSC
ATTN: DEP, J. Bratton
ATTN: DES-G, Mr. Melzer
ATTN: DES-S, M. Plamondon
ATTN: DES-C, R. Henny
ATTN: DE, J. Leech
ATTN: DED

Air Force Systems Command
ATTN: R. Cross
ATTN: DLCAW

ASD
ATTN: Technical Library

Assistant Secretary of the Air Force
Research and Development
ATTN: R. Steere

Deputy Chief of Staff
Research and Development
ATTN: J. Gilbert
ATTN: RDPM
ATTN: RDQPM, V. Vajda
ATTN: RDQSM
ATTN: RDQRM, S. Green
ATTN: RDPS, A. Chiuta

Foreign Technology Division, AFSC
ATTN: PDBG
ATTN: NICD, Library
ATTN: ETDP
ATTN: PDBF, Mr. Spring

USAF/IN
ATTN: IN

Deputy Chief of Staff
Programs and Resources
ATTN: PRE

Rome Air Development Center, AFSC
ATTN: Commander
ATTN: Documents Library/TSLD
ATTN: RBES, R. Mair

SAMSO/DE
ATTN: DEB
ATTN: MMH

SAMSO/DY
ATTN: DYS

SAMSO/MN
ATTN: MMH
ATTN: MNNH

SAMSO/RS
ATTN: RSS/Col G. Dowler

DEPARTMENT OF THE AIR FORCE (Continued)

Strategic Air Command
ATTN: XPFS
ATTN: NRI-STINFO, Library
ATTN: OAI

Director of Conferences (CSEC)
United States Air Force Academy
ATTN: DFCEM, W. Fluhr

DEPARTMENT OF ENERGY

Department of Energy
Albuquerque Operations Office
ATTN: Doc. Con. for Technical Library
ATTN: Director

Department of Energy
Library Branch G-042
ATTN: Doc. Con. for Class Technical Library

Department of Energy
Nevada Operations Office
ATTN: Doc. Con. for Technical Library
ATTN: Director

Division of Military Application
ATTN: Doc. Con. for Test Office

Lawrence Livermore Laboratory
ATTN: Doc. Con. for T. Butkovich
ATTN: Doc. Con. for J. Goudreau
ATTN: Doc. Con. for M. Fernandez
ATTN: Doc. Con. for T. Gold
ATTN: Doc. Con. for J. Thomsen
ATTN: Doc. Con. for R. Dong
ATTN: Doc. Con. for L. Woodruff
ATTN: Doc. Con. for J. Hearst
ATTN: Doc. Con. for J. Cortez
ATTN: Doc. Con. for D. Norris
ATTN: Doc. Con. for Technical Information Department Library
ATTN: Doc. Con. for R. Schock
ATTN: Doc. Con. for J. Kahn

Los Alamos Scientific Laboratory
ATTN: Doc. Con. for A. Davis
ATTN: Doc. Con. for T. Dowler
ATTN: Doc. Con. for G. Spillman
ATTN: Doc. Con. for Reports Library

Oak Ridge National Laboratory
Union Carbide Corporation-Nuclear Division
X-10 Laboratory Records Department
ATTN: Doc. Con. for Civil Def. Res. Proj.
ATTN: Doc. Con. for Technical Library

Sandia Laboratories
Livermore Laboratory
ATTN: Doc. Con. for Library & Security Classification Division

Sandia Laboratories
ATTN: Doc. Con. for W. Caudle
ATTN: Doc. Con. for L. Vortman
ATTN: Doc. Con. for W. Roherty
ATTN: Doc. Con. for L. Hill
ATTN: Doc. Con. for W. Herrmann
ATTN: Doc. Con. for 3141
ATTN: Doc. Con. for A. Chaban

OTHER GOVERNMENT AGENCIES

Central Intelligence Agency
ATTN: RD/SI, Rm. 5G48, Hq. Bldg. for NED/OSI-5G48, Hqs.

Department of the Interior
Bureau of Mines
ATTN: Technical Library

Department of the Interior
U.S. Geological Survey
ATTN: D. Roddy

NASA
Ames Research Center
ATTN: R. Jackson

Office of Nuclear Reactor Regulation
Nuclear Regulatory Commission
ATTN: L. Shao

DEPARTMENT OF DEFENSE CONTRACTORS

Aerospace Corp.
ATTN: L. Selzer
ATTN: P. Mathur
2 cy ATTN: Technical Information Services

Agbabian Associates
ATTN: C. Bagge
ATTN: M. Agbabian

Analytic Services, Inc. (ANSER)
ATTN: G. Hesselbacher

Applied Theory, Inc.
2 cy ATTN: J. Trulio

Artec Associates, Inc.
ATTN: S. Gill

Avco Research & Systems Group
ATTN: J. Atanasoff
ATTN: Code A830
ATTN: D. Henderson
ATTN: W. Broding

Battelle Memorial Institute
ATTN: Technical Library
ATTN: R. Klingsmith

BDM Corp.
ATTN: Corporate Library
ATTN: A. Lavagnino

BDM Corp.
ATTN: R. Hensley

Bell Telephone Laboratories
ATTN: J. White

Boeing Co.
ATTN: K. Friddell
ATTN: Aerospace Library
ATTN: R. Dyrdahl
ATTN: R. Carlson
ATTN: R. Hager
ATTN: J. Bodwell
ATTN: J. Wooster
ATTN: R. Holmes

DEPARTMENT OF DEFENSE CONTRACTORS (Continued)

Brown Engineering Company, Inc.
ATTN: M. Patel

California Institute of Technology
ATTN: T. Ahrens

California Research & Technology, Inc.
ATTN: K. Kreyenhagen
ATTN: Technical Library
ATTN: S. Shuster

Calspan Corp.
ATTN: Technical Library

Center for Planning & Rsch., Inc.
ATTN: R. Shnider

Civil/Nuclear Systems Corp.
ATTN: R. Crawford

University of Dayton
Industrial Security Super KL-505
ATTN: H. Swift

University of Denver
Colorado Seminary
Denver Research Institute
ATTN: Sec. Officer for J. Wisotski

EG&G Washington Analytical Services Center, Inc.
ATTN: Library
ATTN: Director

Electric Power Research Institute
ATTN: G. Sliter

Electromechanical Sys. of New Mexico, Inc.
ATTN: R. Shunk

Engineering Decision Analysis Co., Inc.
ATTN: R. Kennedy

Franklin Institute
ATTN: Z. Zudans

Gard, Inc.
ATTN: G. Neidhardt

General Dynamics Corp.
Pomona Division
ATTN: K. Anderson

General Dynamics Corp.
Electric Boat Division
ATTN: M. Pakstys

General Electric Co.
Space Division
ATTN: M. Bortner

General Electric Co.
Re-Entry & Environmental Systems Div.
ATTN: A. Ross

General Electric Company-TEMPO
Center for Advanced Studies
ATTN: DASIAC

DEPARTMENT OF DEFENSE CONTRACTORS (Continued)

General Research Corp.
Santa Barbara Division
ATTN: B. Alexander

Geocenters, Inc.
ATTN: E. Marram

H-Tech Laboratories, Inc.
ATTN: B. Hartenbaum

Honeywell, Inc.
Defense Systems Division
ATTN: T. Helvig

IIT Research Institute
ATTN: Documents Library
ATTN: R. Welch

University of Illinois
ATTN: A. Ang

Institute for Defense Analyses
ATTN: Classified Library
ATTN: Director

J. H. Wiggins Co., Inc.
ATTN: J. Collins

Kaman AviDyne
Division of Kaman Sciences Corp.
ATTN: N. Hobbs
ATTN: E. Criscione
ATTN: Technical Library
ATTN: G. Zartarian

Kaman Sciences Corp.
ATTN: P. Ellis
ATTN: Library
ATTN: F. Shelton
ATTN: D. Sachs

Karagozian and Case
ATTN: J. Karagozian

Lockheed Missiles & Space Co., Inc.
ATTN: TIC-Library

Lockheed Missiles and Space Co., Inc.
ATTN: T. Geers
ATTN: B. Almroth

Lovelace Foundation for Medical Education & Research
ATTN: R. Jones

Martin Marietta Corp.
Orlando Division
ATTN: G. Fotieo
ATTN: A. Cowan

University of Massachusetts
ATTN: W. Nash

McDonnell Douglas Corp.
ATTN: R. Halprin

McMillan Science Associates, Inc.
ATTN: W. McMillian

DEPARTMENT OF DEFENSE CONTRACTORS (Continued)

Merritt CASES, Inc.
ATTN: J. Merritt

Meteorology Research, Inc.
ATTN: W. Green

Mitre Corp.
ATTN: Director

University of New Mexico
Dept. of Campus Security and Police
ATTN: G. Triandafalidis

University of New Mexico
Civil Engineering Rsch. Facility
ATTN: N. Baum
ATTN: D. Calhoun

Nathan M. Newmark Consulting Engineering Services
ATTN: N. Newmark
ATTN: W. Hall

University of Oklahoma
Research Institute
ATTN: J. Thompson

Pacifica Technology
ATTN: R. Allen
ATTN: R. Bjork
ATTN: G. Kent

Physics International Co.
ATTN: F. Sauer
ATTN: C. Vincent
ATTN: R. Swift
ATTN: E. Moore
ATTN: D. Orphal
ATTN: L. Behrmann
ATTN: Technical Library

University of Pittsburgh
School of Engineering
ATTN: M. Willims, Jr.

Prototype Development Associates, Inc.
ATTN: T. McKinley

R & D Associates
ATTN: A. Latter
ATTN: P. Rausch
ATTN: C. Knowles
ATTN: W. Wright, Jr.
ATTN: H. Brode
ATTN: J. Carpenter
ATTN: J. Lewis
ATTN: Technical Information Center
ATTN: A. Fields
ATTN: R. Port

R & D Associates
ATTN: H. Cooper

Rand Corp.
ATTN: A. Laupa
ATTN: Library
ATTN: C. Mow

Science Applications, Inc.
ATTN: Technical Library

DEPARTMENT OF DEFENSE CONTRACTORS (Continued)

Science Applications, Inc.
ATTN: S. Oston

Science Applications, Inc.
ATTN: R. Hoffmann
ATTN: D. Maxwell
ATTN: D. Bernstein

Science Applications, Inc.
ATTN: W. Layson
ATTN: B. Chambers

Southwest Research Institute
ATTN: W. Baker
ATTN: A. Wenzel

SRI International
ATTN: W. Wilkinson
ATTN: G. Abrahamson

Systems, Science & Software, Inc.
ATTN: R. Sedgewick
ATTN: D. Grine
ATTN: T. Cherry
ATTN: Library
ATTN: T. Riney

Terra Tek, Inc.
ATTN: Library
ATTN: S. Green
ATTN: A. Jones

Tetra Tech, Inc.
ATTN: L. Hwang
ATTN: Library

Texas A & M University System
c/o Texas A & M Research Foundation
ATTN: H. Coyle

TRW Defense & Space Sys. Group
ATTN: A. Narevsky
ATTN: N. Lipner
ATTN: D. Jortner
ATTN: P. Bhutta
ATTN: B. Sussholtz
ATTN: A. Feldman
ATTN: Tech. Info. Center
ATTN: J. Farrell
ATTN: J. Chiu
ATTN: A. Soux
2 cy ATTN: P. Dai

TRW Defense & Space Sys. Group
San Bernardino Operations
ATTN: G. Hulcher
ATTN: F. Pieper
ATTN: E. Wong

Universal Analytics, Inc.
ATTN: E. Field

The Eric H. Wang Civil Engineering Rsch. Fac.
ATTN: L. Bickle
ATTN: N. Baum

Weidlinger Assoc., Consulting Engineers
ATTN: J. McCormick
ATTN: M. Baron

DEPARTMENT OF DEFENSE CONTRACTORS (Continued)

Weidlinger Assoc., Consulting Engineers
ATTN: J. Isenberg

Westinghouse Electric Corp.
Maring Division
ATTN: W. Volz

DEPARTMENT OF DEFENSE CONTRACTORS (Continued)

Westinghouse Electric Corp.
ATTN: F. Petkevicivs